Abstracts of Papers Submitted to the Fifth ANS Topical Meeting on the Technology of Fusion Energy by the University of Wisconsin Fusion Engineering Program

various authors

October 1982

UWFDM-489

Meeting held in Knoxville, TN, 26-28 April 1983.

FUSION TECHNOLOGY INSTITUTE

UNIVERSITY OF WISCONSIN

MADISON WISCONSIN

Abstracts of Papers Submitted to the Fifth ANS Topical Meeting on the Technology of Fusion Energy by the University of Wisconsin Fusion Engineering Program

various authors

Fusion Technology Institute
University of Wisconsin
1500 Engineering Drive
Madison, WI 53706

http://fti.neep.wisc.edu

October 1982

UWFDM-489

Meeting held in Knoxville, TN, 26-28 April 1983.

ABSTRACTS OF PAPERS SUBMITTED TO THE FIFTH ANS TOPICAL MEETING ON THE TECHNOLOGY OF FUSION ENERGY BY THE UNIVERSITY OF WISCONSIN FUSION ENGINEERING PROGRAM - OCTOBER 1982

Meeting to be held in Knoxville, TN, 26-28 April 1983

Fusion Engineering Program
Nuclear Engineering Department
University of Wisconsin
Madison, Wisconsin 53706

October 1982

UWFDM-489

TABLE OF CONTENTS

NEUTRON ACTIVATION AND SHIELDING OF THE LIGHT ION FUSION TARGET DEVELOPMENT FACILITY

K.J. O'Brien, A.M. White, and G.A. Moses (University of Wisconsin)

The light ion fusion target development facility [1] (TDF) is an experimental nuclear facility operated at an average power level of 23 kW (ten 200 MJ shots per day). It also requires easy access for maintenance. To accomplish this, low activation materials, aluminum, have been used for the target chamber, and a borated water shield fills the space occupied by the magnetically insulated transmission lines of the pulsed power machine. This arrangement is shown schematically in Fig. 1, where the water level is shown lowered to allow access through the top end cap of the target chamber. The water level is raised during operation.

Neutron activation calculations were performed for the first wall candidate materials and the resultant dose levels at the first wall are summarized in Table 1. It is seen that Al and Cu-Be are much preferred over the Fe based alloys and Ti. Hands-on maintenance is possible after 1 week for the Al target chamber whereas this is probably not possible for the Fe based alloys. The water shield very effectively attenuates the neutrons and gammas during operation.

Following a target explosion, the vibrating target chamber creates acoustic waves in the water shield. To attenuate these waves before they reach the water filled section of the pulsed power generator, air bubbles are introduced into the shield region, see Fig. 1. Calculations have been performed to determine the reflection, attenuation, and transmission of acoustic waves from bubble filled regions. A result of these calculations is shown in Fig. 2 where the transmission fraction is plotted as a function of the bubble void fraction for different bubble screen widths. Bubble "screens" will very effectively block the acoustic waves from propagating outward, but if not properly designed, they will simply reflect the waves back inward toward the target chamber. Hence the bubble screen detailed design is important to the achievement of the desired effect.

This work was performed for Sandia National Laboratory under contract number DE-AS08-81DP40161.

References

1. G.A. Moses et al., "Light Ion Fusion Target Development Facility Pre-Conceptual Design," these proceedings.

Table 1. Dose at First Wall (mr/hr)

Material	Time After Shutdown 0	1 day	1 week
Al 6061	2,100	260	1.65
HT-9	489	114	101
SS-304	481	109	105
Ti-6Al-4V	515	177	66
Cu-Be	1,060	204	7.

Figure 1

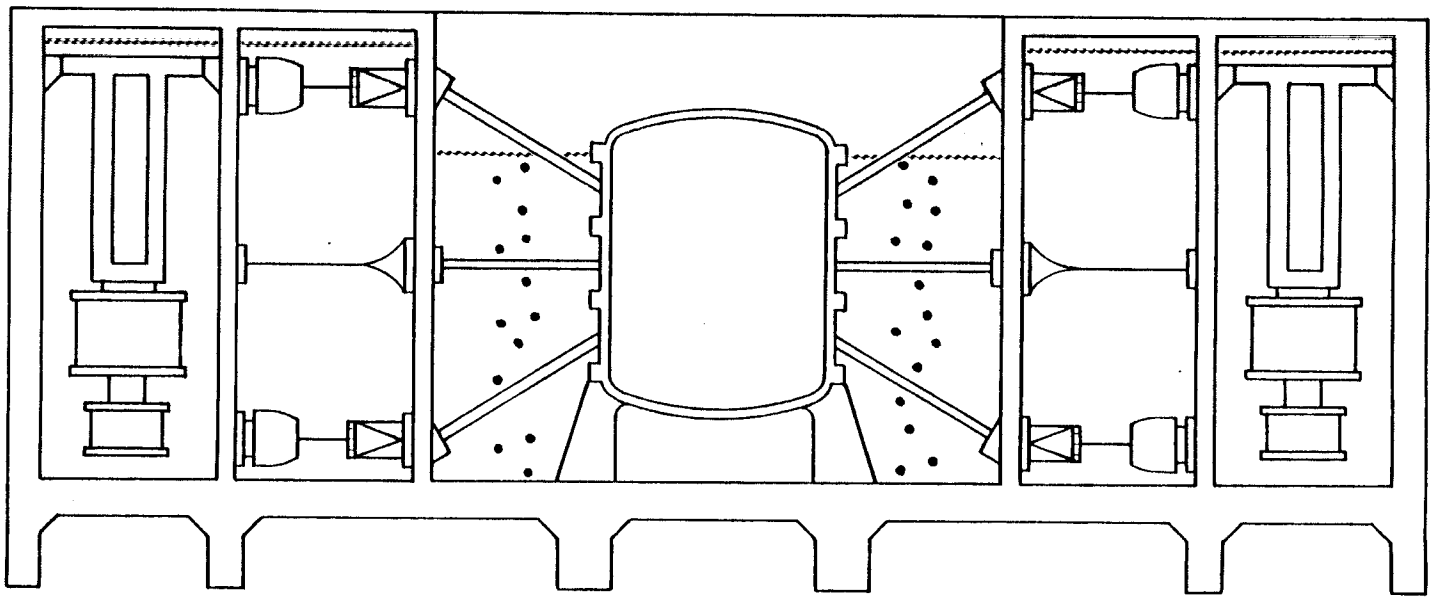

Figure 2

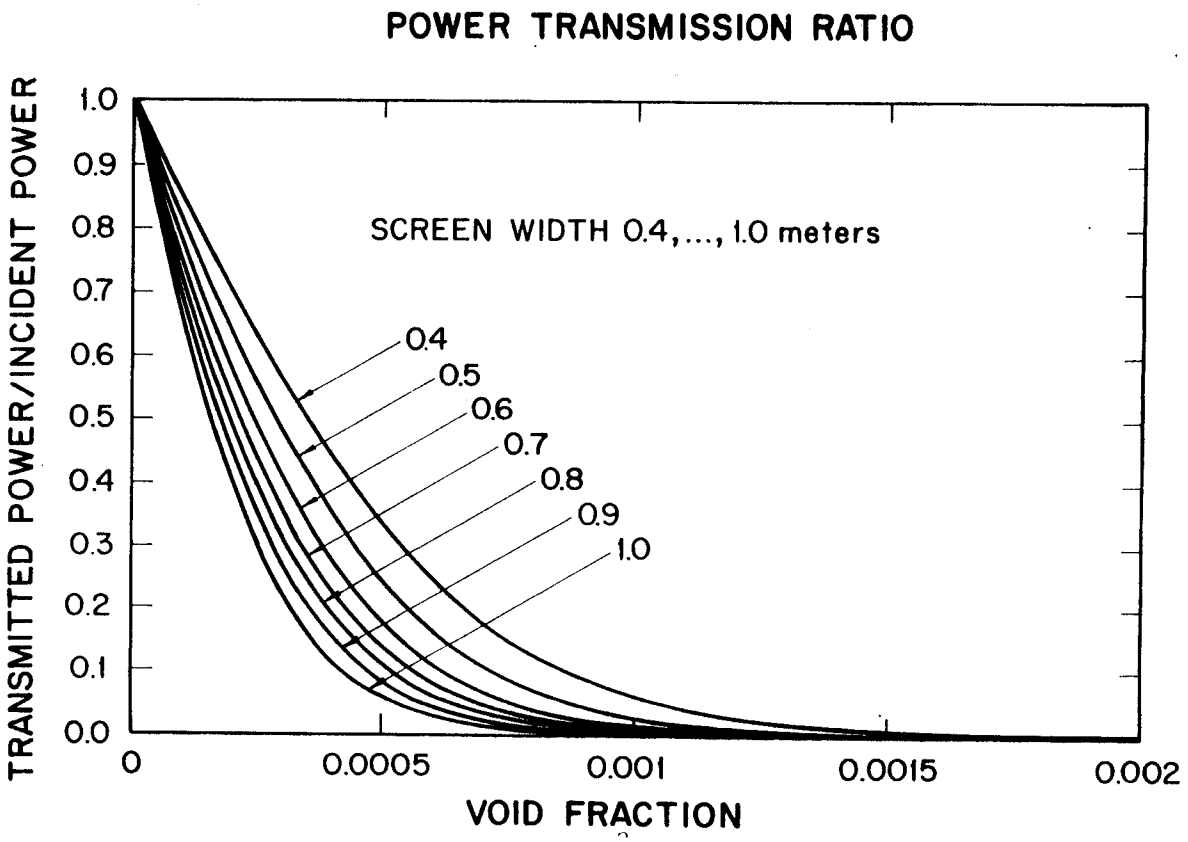

FIRST WALL MATERIALS SELECTION FOR THE LIGHT ION FUSION TARGET DEVELOPMENT FACILITY

R.R. Peterson, E.G. Lovell, K.J. Lee, R.L. Engelstad,
G.L. Kulcinski, and G.A. Moses (University of Wisconsin)

The light ion fusion target development facility [1] (TDF) is an experimental facility designed to test high yield light ion beam driven ICF targets. Its operation will follow the successful completion of experiments on PBFA-II. A critical element in the design of the facility is the reaction chamber in which the fusion micro-explosion must be contained. The reaction chamber walls consist of panels, supported from behind by a structural frame. The calculated mechanical response of this structure is reported by Lovell and Engelstad in these proceedings [2].

In this paper, a survey of seven common metal alloys is made with regard to their viability as a first wall material for the TDF. The criteria include: cost, fatigue strength, thermal shock resistance, neutron activation, and compatibility with N_2 gas. The materials are listed in Table 1 with their physical properties. Radiation damage resistance and heat transfer to a coolant were not considered important because the TDF shot rate is only 10 shots/day and the structure is completely immersed in a water shield at room temperature.

Figure 1 shows typical results for Al 6061, where the first wall panel thickness was determined to be 3 cm for a lifetime of 10^4 shots. All of the candidate materials were found to be acceptable as a first wall material with aluminum being chosen as the best material. The two most important criteria were thermal shock resistance and neutron activation. The latter is discussed by O'Brien et al. in these proceedings [3]. Thermal shock resistance is a combination of high conductivity and low thermal expansion. The high strength alloys like steel and Ti have poor thermal shock resistance and this fact outweighs their great strength. Hence the lower strength Al is the best candidate.

This work was supported by Sandia National Laboratory under contract number DE-AS08-81DP40161.

References

1. G.A. Moses et al., "Light Ion Fusion Target Development Facility Pre-Conceptual Design," these proceedings.

2. E.G. Lovell and R.L. Engelstad, "Dynamic Stress Analysis of the Light Ion Fusion Target Development Facility Reaction Chamber," these proceedings.

3. K.J. O'Brien, A.M. White, and G.A. Moses, "Neutron Activation and Shielding of the Light Ion Fusion Target Development Facility," these proceedings.

Table I Thermal and Mechanical Properties of Selected Metal Alloys (Room Temperature)

Metal Alloys	Temper Type	Density (ρ)	Specific Heat (C_p)	Thermal Conductivity (K)	Diffusivity ($K/\rho C_p$)	Melting Point	Thermal Expansion Coefficient (α)	Poisson's Ratio (ν)	Young's Modulus (E)	Yield Strength (σ_y)	$\frac{K(1-\nu)}{\alpha E}$	$\frac{2\sigma_y K(1-\nu)}{\alpha E}$
		g/cm^3	J/g-°K	W/m-°K	cm^2/sec	°C	10^{-6}/°K		GPa (KSI)	MPa (KSI)	W/m-MPa	W/m
Al 6061	T6	2.70	0.90	167	0.687	652	23.6	0.33	69 (10,000)	276 (40)	68.7	37920
Al 5086	H34	2.66	0.90	127	0.530	640	23.8	0.33	71 (10,300)	255 (37)	50	25680
304 SS	Annealed	8.0	0.50	16.2	0.0405	1375 ~ 1440	17.2	0.29	193 (28,000)	255 (36.9)	3.4	1750
HT-9		7.75	0.59	29	0.0634	1427 ~ 1482	10.6	0.265	200 (29,000)	442 (64)	10	8870
Ti-6Al-4V	Solution Treated and Aged Bar	4.43	0.67	6.8	0.0222	1660	8.8	0.33	110 (16,000)	1070 (155)	4.7	10030
Cu-Be (C17200)	TB00	8.25	0.42	118	0.340	980	16.7	0.3	128 (18,500)	283 (41)	38.7	21890
Cu-Be (C17600)	TB00	8.75	0.42	230	0.626	1068	16.7	0.3	128 (18,500)	173 (25)	75.5	26050

(Refs.: 1) Metals Handbook, 9th ed., American Society for Metals, Metals Park, Ohio (1979).
2) Structural Alloys Handbook, Battelle's Columbus Laboratories, Columbus, Ohio (1981).
3) Aerospace Structural metals Handbook, Mechanical Properties Data Center, Belfour Stulen, Inc., Traverse City, Michigan (1975, 1981).
4) C.C. Baker et al., "STARFIRE - A Commercial Tokamak Fusion Power Plant Study," Argonne National Laboratory (1980).

Fig. 1

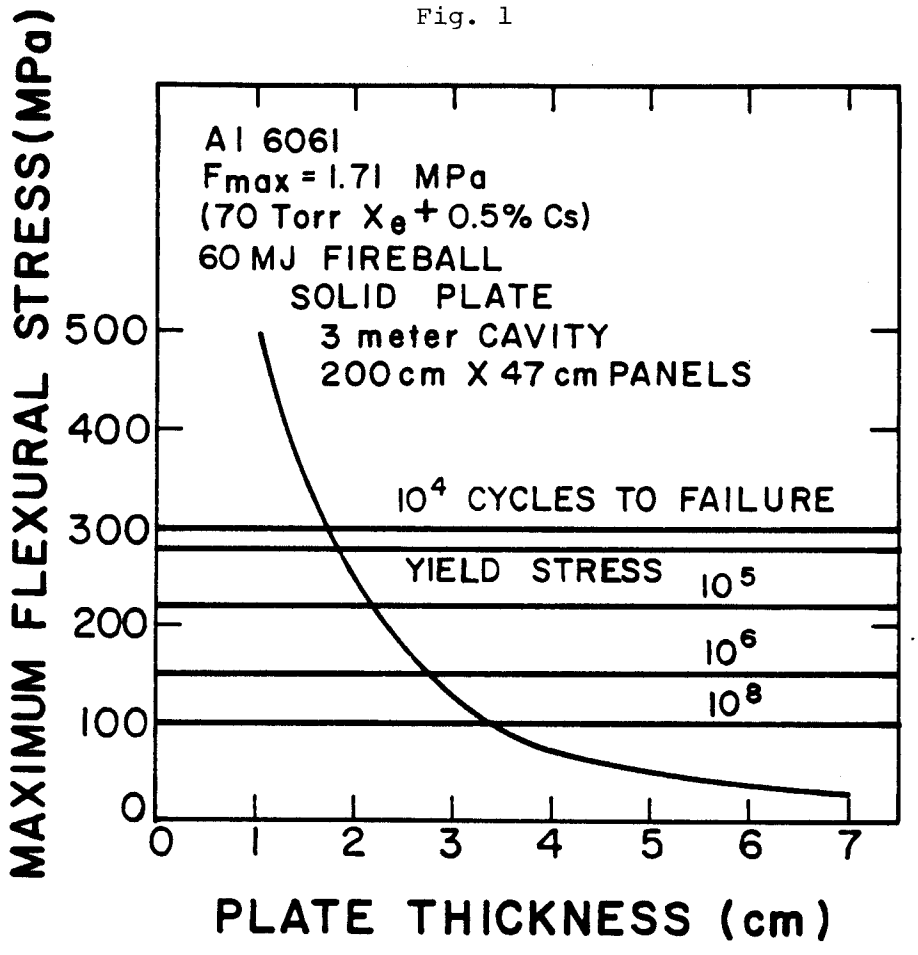

TARGET EXPLOSION GENERATED FIREBALLS IN THE NITROGEN FILLED TARGET CHAMBER OF THE LIGHT ION FUSION TARGET DEVELOPMENT FACILITY

R.R. Peterson and G.A. Moses (University of Wisconsin)

The response of a nitrogen target chamber gas to fusion target explosions is considered for the light ion beam driven target development facility (TDF). Targets are considered with yields of 200 MJ, 400 MJ and 800 MJ. In each of these cases, 70% of the yield is assumed to be in hard x-rays and neutrons with the remainder being soft x-rays and target debris ions. These ions are stopped in a very short distance in the nitrogen gas which we assume has a density of 7.07×10^{17} N_2 molecules/cm^3. We have assumed that the soft x-rays are absorbed in 30 cm of target chamber gas. The energy of the soft x-rays and ions thus creates a hot spherical "fireball" 30 cm in radius which can propagate to the first wall of the target chamber, subjecting the wall to fluxes of low energy photons and shock pressure pulses.

The propagation of these fireballs has been simulated with a Lagrangian radiation transport hydrodynamics computer code FIRE [1], which uses equations of state and optical data for N_2 generated with the computer code MIXERG [2]. N_2 was chosen as a target chamber gas for its compatibility with first wall materials, for the ease in handling the tritium-nitrogen compounds, and for the ability to efficiently create laser guided plasma channels in N_2 [3]. The results of these simulations in N_2 for yields of 200 MJ, 400 MJ and 800 MJ are shown in Table I for a 3 meter radius target chamber. The heat flux and shock pressure at the first wall for a 200 MJ shot are shown in Figure 1. One should notice that in all cases only a very small fraction of the fireball energy escapes as radiant energy but that the shock pressures are large.

These simulations have shown that the first wall must mainly be protected against the mechanical shock of the fireball because the heat loads are low in all three cases. The yield strength of the wall is not exceeded by the higher yield shots so that a wall designed for 15,000 shots of 200 MJ will withstand a few at 400 and 800 MJ.

References

1. T.J. McCarville, R.R. Peterson and G.A. Moses, "Improvements in the FIRE Code for Simulating the Response of Cavity Gases to Inertial Confinement Fusion Target Explosions," University of Wisconsin Fusion Engineering Program Report UWFDM-407 (Feb. 1982); accepted for publication in Computer Physics Communications.
2. R.R. Peterson and G.A. Moses, "MIXERG - An Equation of State and Opacity Computer Code," University of Wisconsin Fusion Engineering Program Report UWFDM-464 (March 1982); accepted for publication in Computer Physics Communications.
3. R.R. Peterson, G.A. Moses and G.W. Cooper, "Cavity Gas Analysis for Light Ion Beam Fusion Reactors," Nuclear Technology/Fusion 1, 377 (July 1981).

Table I. Fireball Propagation in TDF Target Chamber

Target Yield (MJ)	Initial Fireball Energy (MJ)	Chamber Radius (m)	Chamber Gas	Gas Density (atoms/cm^3)	Max. Wall Pressure (MPa)	Energy Radiated to Wall (MJ)
200	60	3	N_2	1.4×10^{18}	1.38 @ 0.39 msec	2.3 @ 1.5 msec
400	120	3	N_2	1.4×10^{18}	3.06 @ 0.29 msec	7.4 @ 1.5 msec
800	240	3	N_2	1.4×10^{18}	6.32 @ 0.21 msec	28.8 @ 1.5 msec

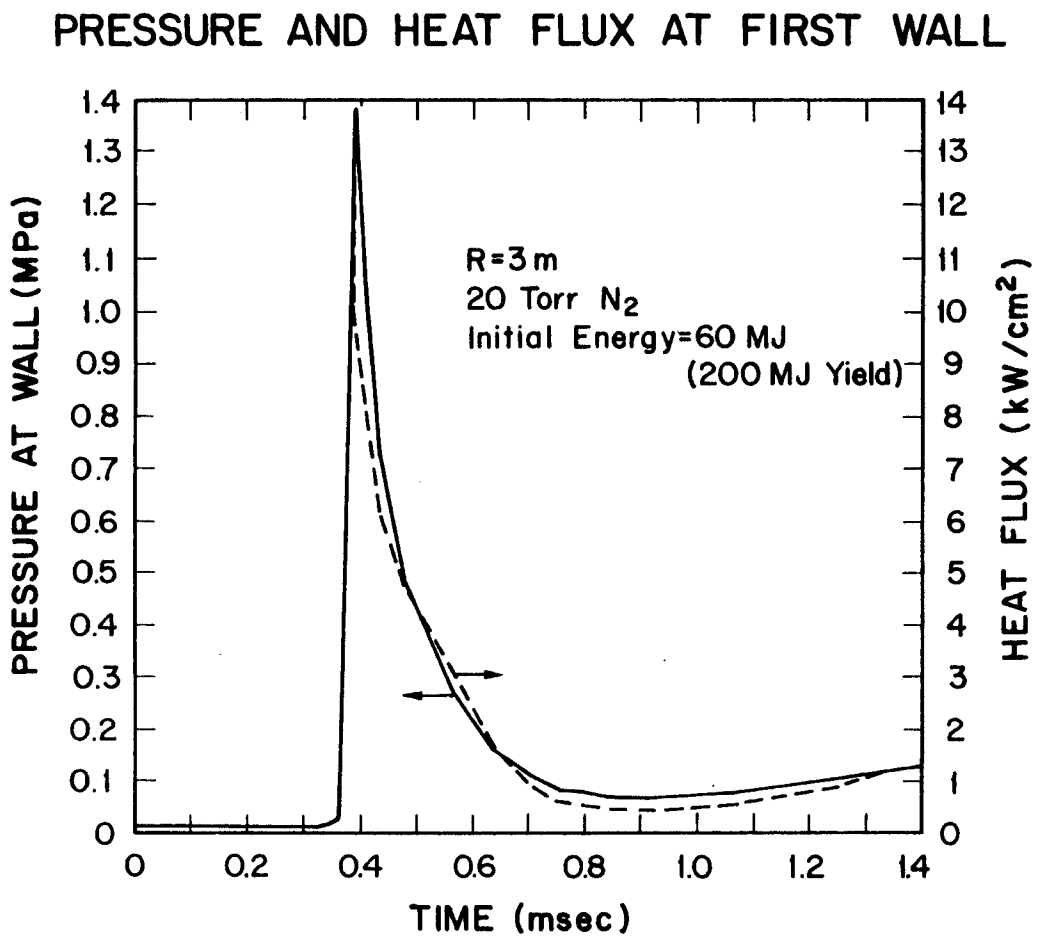

Figure 1. Heat flux and shock pressure at a 3 meter radius first wall due to a 200 MJ shot in N_2.

LIGHT ION FUSION TARGET DEVELOPMENT FACILITY PRE-CONCEPTUAL DESIGN

G.A. Moses, R.R. Peterson, R.L. Engelstad, E.G. Lovell, G.L. Kulcinski, K.J. O'Brien, A.M. White, J.J. Watrous (University of Wisconsin)
D.L. Cook (Sandia National Laboratory)

The light ion fusion target development facility (TDF) will be used to test high yield (~ 50-200 MJ) light ion beam driven ICF targets. This facility has a designed lifetime of 15,000 shots over five years (10 shots/day) and is expected to be built following the successful operation of PBFA-II. This places the TDF operation in the 1990-95 time frame and demands that the design rely upon modest extrapolations beyond state-of-the-art technology. A conceptual drawing of the TDF is shown in Fig. 1 and a list of its operating parameters are given in Table 1.

The pulsed power generator for TDF is a modest extension of PBFA-I and II technology to higher levels of stored energy and more power per beam line. There are 40 individual diodes and 20 return current terminals located behind the reaction chamber first wall with 8 MJ of EM pulse energy delivered to the diodes.

The reaction chamber is filled with 20 torr of N_2 gas to support the formation of z-pinch plasma channels. These plasma channels are formed by first firing a laser along the channel path to pre-ionize or excite the cavity gas and then discharging a capacitor into the channels. Ions are focused into these plasma channels at the first wall and propagate through them to the target. The exploding target creates a fireball in the N_2 gas and this fireball creates a transient overpressure and heat flux at the first wall. This overpressure is accommodated by a first wall design consisting of panels supported from behind by a tubular frame. The first wall material is Al 6061 and was chosen from a study of seven different metal alloys (Al 6061, Al 5086, Cu-Be C17200, Cu-Be C17600, HT-9, SS 304, Ti-6Al-4V) as the best for meeting the combined criteria of: strength, thermal shock resistance, neutron activation and cost. The first wall is conservatively designed to withstand both the maximum possible overpressure as well as the maximum possible heat flux from a 200 MJ target explosion for 15,000 shots. These two conditions will in practice never occur simultaneously and the nominal expected values for 20 torr of N_2 gas are comfortably bounded by these extremes.

The reaction chamber is shielded by a borated water shield that very effectively attenuates the neutron and gamma fluxes. It can be easily drained to gain access to the target chamber. Acoustic waves in the water, created by the vibrating chamber following an explosion, are attenuated by introducing air bubbles in the water shield in a precise way, so as to avoid reflection back toward the target chamber.

This work was supported by Sandia National Laboratory under contract number DE-AS08-81DP40161.

Table 1. Target Development Facility Operating Parameters

Target	
Energy requirement	≤ 4 MJ
Yield	50-200 MJ
Radius	0.5 cm
Driver	
Energy in store	15 MJ
Energy at diodes	8 MJ
Diode voltage	4-30 MV
Power at diodes	200 TW
Pulse width at diodes	40 ns
Plasma Channels	
Length	4. m
Current	85 kA
Number	60
Radius at firing time	0.5 cm
Cavity Gas	
Type	20 Torr N_2
Cavity	
Shape	cylindrical
Height	6 m
Diameter	6 m
Max. overpressure at wall	1.7 MPa
Max. energy flux	53 J/cm^2
Shot rate	10/day
First Wall	
Material	Al 6061
Thickness	3 cm
Design	Solid plate panels supported by frame
Number of panels	60
Panel Width	0.47 cm
Panel height	2 m
Fatigue life	1.5 x 10^4
Shield	
Type	Borated water with air bubbles to suppress acoustic waves

Figure 1 Light Ion Beam Target Development Facility

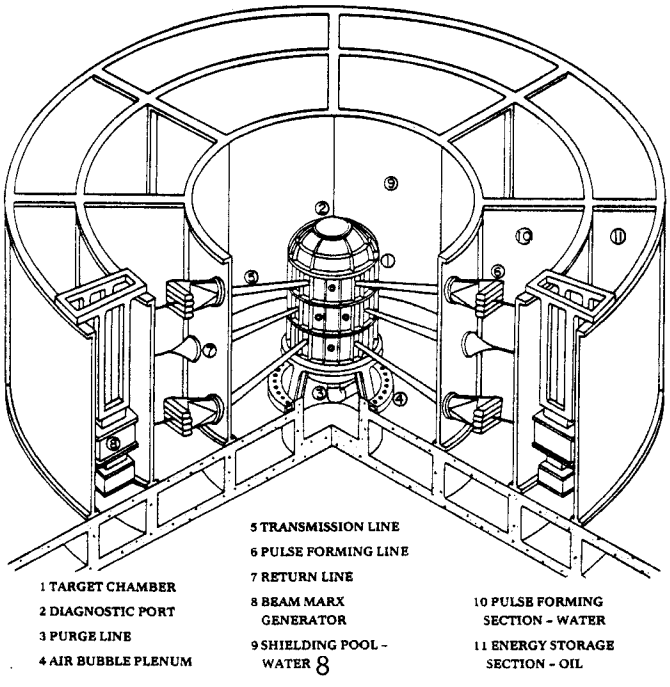

DYNAMIC STRESS ANALYSIS OF LIGHT ION FUSION TARGET DEVELOPMENT FACILITY REACTION CHAMBERS

Edward G. Lovell
Roxann L. Engelstad
University of Wisconsin-Madison

The reaction chamber of the proposed Target Development Facility shown in the figure below is a capped cylindrical shell, reinforced by circumferential ribs and axial stringers. The most important sources of stress are heat flux and mechanical shock transmitted by the cavity gas. The results reported in this paper focus on the mechanical overpressure problem and include details of analysis methods and associated design considerations for the structural system.

For a design using a large number of stringers, the sections of unsupported shell wall can be considered to be very shallow curved plates. As a first approximation, curvature effects are ignored and flexural stress and deflection calculations are based upon flat plate theory. The dynamic response of wall plate components is determined by multiplying the quasi-static stress and deflection by dynamic load factors or dynamic load functions. Such amplifiers depend upon the characteristics of the pressure pulse (rise time and decay strength), natural vibration fre-

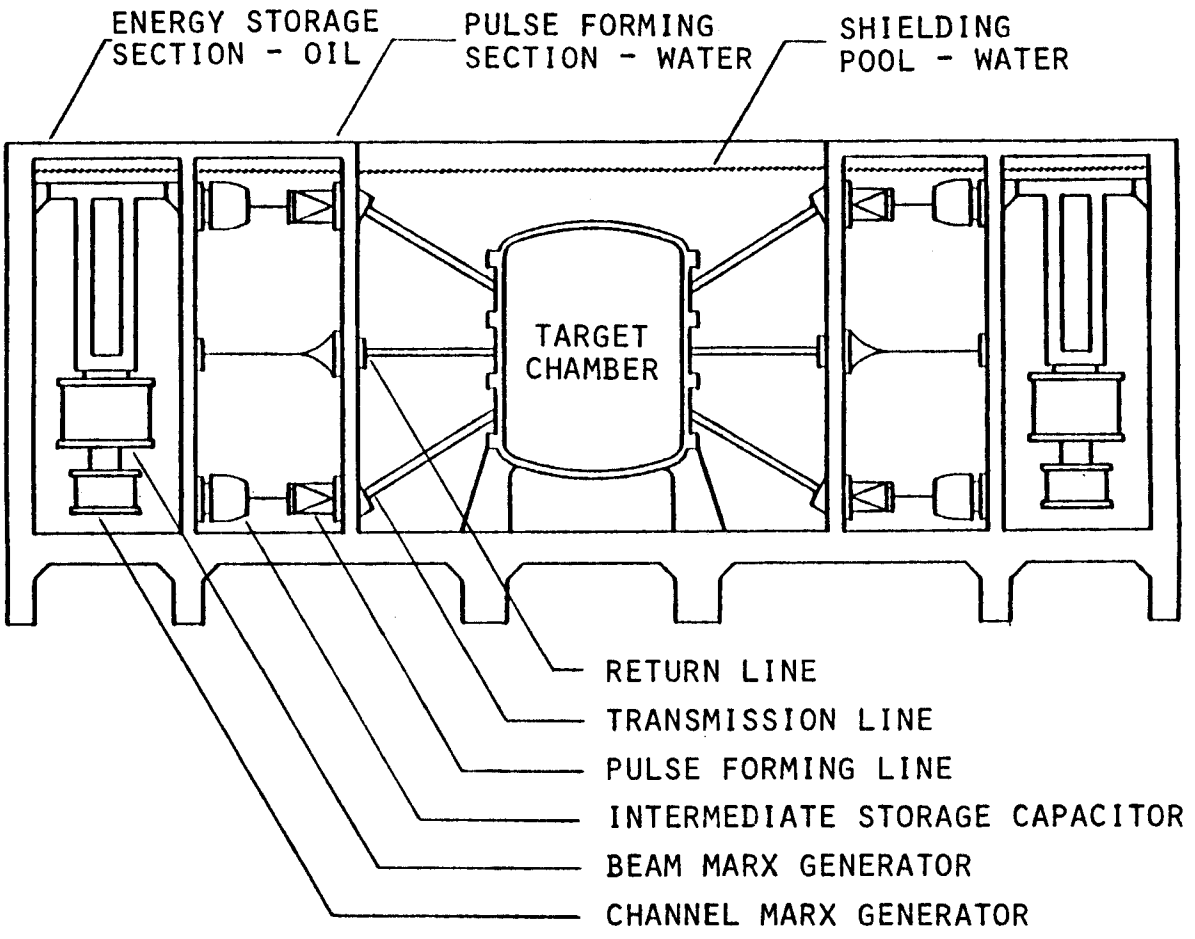

quencies of the plate, wall material and level of damping. A computer code has been developed for this purpose and has also been coupled with a thermal stress code for the determination of the total stress history in the chamber wall. An improved shell theory model has also been developed which includes the effects of curvature, in-plane (membrane) forces, twist and shell flexural stresses. For shallow panels (e.g. subtending 9°) the differences between shell theory and flat plate theory are minor.

The response results shown correspond to the specific case of a 200 MJ target yield and xenon cavity gas at 70 torr with 0.5% cesium. The wall component is solid aluminum with 2.5% critical damping and height, width and thickness of 200, 47 and 3 cm, respectively. The fundamental frequency of this component in flexural is 768.5 Hz and the overpressure is 1.71 MPa. The circumferential stress history is shown for a point at the center of the concave surface of the shell. The first flexural stress peak is compressive and adds directly to the compressive thermal stress from the heat flux. Near the ribs and stringers, flexural stress will initially be tensile and will be counteracted by compressive thermal stress.

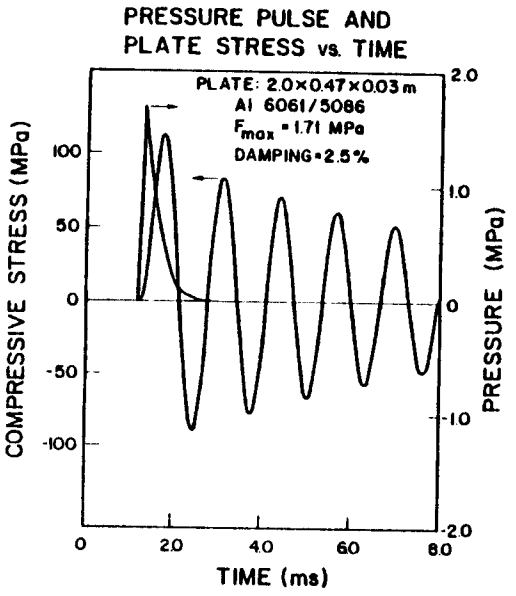

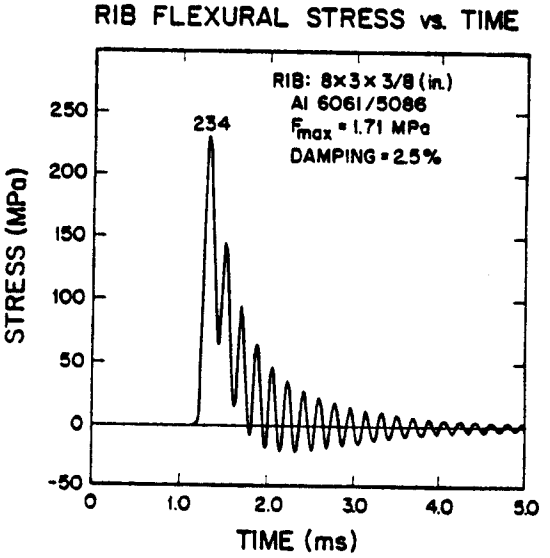

The rib and stringer analysis involves techniques which are very similar to that used for the plates. The design primarily involves the determination of cross section characteristics such that mechanical stresses are within acceptable limits and deflections are not excessive. A typical stress history is shown for an aluminum rib with a hollow rectangular cross section.

The procedures developed and corresponding numerical results indicate that a first wall structural system can be designed to carry the dynamic pressures and heat flux anticipated in this facility.

This work was supported by Sandia National Laboratories, Albuquerque, N.M.

STREAMING AND SHIELDING ANALYSIS FOR THE NBI SYSTEM OF TDF

M.E. Sawan
University of Wisconsin
Department of Nuclear Engineering
Madison, Wisconsin 53706

Fusion reactors are required to accommodate a variety of penetrations. Proper shielding is required to protect the vital components in the penetration from excessive radiation damage caused by radiation streaming. Different penetrations exist in the Technology Development Facility (TDF) tandem mirror fusion device. A major penetration in the central cell, where most of the fusion neutrons are produced, is the neutral beam injector (NBI) duct which has a duct opening size at the first wall of 0.3 m x 0.6 m. There are four such penetrations at each end of the central cell and they must fit between the central cell solenoids. Radiation streaming can lead to adverse effects in the superconducting magnets and hence, it is essential to provide sufficient shielding between the duct wall and the magnets. In this work, detailed streaming and shielding analysis for the NBI system of TDF is presented.

The MCNP continuous energy coupled neutron gamma Monte Carlo code was used to model the reactor geometry. The neutron source was sampled from the neutron linear source density distribution along the machine axis. The source density was normalized to a central cell neutron wall loading of 2 MW/m^2 at a radius of 0.25 m. A trapping surface was located at the entrance surface to the NBI duct. At this surface all particles entering the duct were counted according to energy and angle bins. The results were stored to serve as source distributions in later modelling of the NBI duct itself. Cross section data based on ENDF/B-V were used in the calculations. 3.1×10^{17} neutrons and 5.6×10^{16} gamma photons were found to stream per second into the duct with average energies of 6.9 and 1.44 MeV, respectively. The angular distribution of streaming radiation reveals that a large fraction of it will go directly towards the ion source at the end of the duct.

Fig. 1 gives the geometrical model used for modelling the NBI system in TDF. Only the corner of the central cell solenoid, which has the largest radiaton effects from streaming particles, was modelled. The magnet case, cryostat and vacuum vessel surrounding the winding pack have a total effective stainless steel thickness of 0.125 m which was modelled in the calculation. The shield consists of 56 v/o Fe-1422, 26 v/o B_4C, 14 v/o Pb and 4 v/o H_2O. The option of replacing Fe-1422 by tungsten in the 0.35 m thick shield zone at the magnet corner was considered to provide adequate magnet shielding. The deflection magnet, aluminum cryopanels and 0.05 m thick superconductive shield were included in the model. The MACOR insulator in the ion source is concealed from direct line of sight of neutrons by an effective 0.1 m thick stainless steel structure. An extra 0.1 m thick tungsten shield, with holes allowing for the beams to go through, is used to provide adequate radiation protection for the MACOR. The NBI system model, together with the neutron and gamma

surface sources at the duct opening, was used in the three-dimensional Monte Carlo calculation. An angular source biasing technique was used to provide statistically adequate estimates of the quantities of interest. An MCNP run of 50,000 histories was carried out resulting in statistical uncertainties less than 20%.

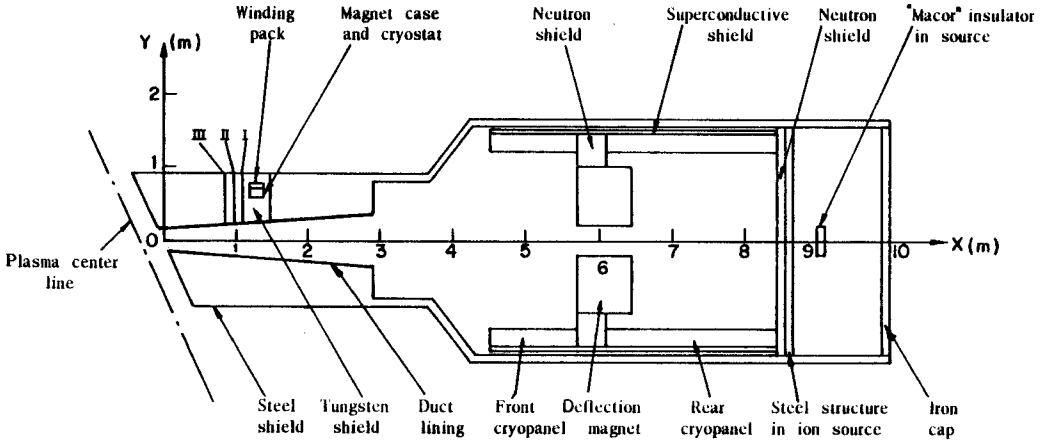

Fig. 1 Geometrical Model for the NBI System in TDF

The shielding requirements for the superconducting central cell solenoids are determined by a number of radiation limits. The dpa rate in the copper stabilizer should not exceed 5.5×10^{-5} dpa per full power year (FPY). The radiation dose in the polyimide insulator should not exceed 5×10^{9} rad after an estimated reactor lifetime of 5.4 FPY. The limit on the peak heat load is considered to be 0.06 mW/cm^3. Since in this analysis only radiation effects resulting from radiation streaming into the NBI duct are considered, a factor of two lower radiation limits are required to allow for the extra contribution through the magnet bulk shield. Using tungsten shield over a length of 0.6 m of the duct at the magnet corner (option III in Fig. 1) was found to provide adequate magnet shielding. Acceptable values for the peak heat load in the superconductive shield and aluminum cryopanels of 0.47 and 0.96 mW/cm^3, respectively, were obtained. The dose rate in the MACOR insulator of the ion source was found to be 2.17×10^{8} rad/FPY implying that it will last 2.77 FPY as far as radiation is concerned. In conclusion, the NBI penetration shield design in TDF will provide adequate protection for the central cell superconducting magnets and other vital components in the system.

Funding for this work was provided by the U.S. Department of Energy.

Effect of Temperature on Magnetic Field Perturbation from the Ferromagnetic Blankets in MARS

H. Attaya and G.L. Kulcinski
Nuclear Engineering Department, University of Wisconsin
Madison, Wisconsin 53706

Because of its high resistance to irradiation damage, the ferritic steel alloy HT-9 is proposed for the structural material in the MARS blanket. Many questions, however, have been raised about the interaction of this ferromagnetic material with the magnetic field. One of these questions arises from the fact that the magnetization is a function of the temperature and because the temperature (hence the magnetization of the HT-9) in the blanket varies with position. Hence, the question addressed here is "will that variation of the magnetization produce any magnetic effect in the plasma region?"

Temperature and Magnetization Distribution in MARS Blanket. In the MARS blanket the LiPb coolant enters from the top of the blanket at 330°C and leaves the bottom of the blanket at 500°C. The temperature T at any angle θ is

$$T = 330 + (500-330)\ \theta/\pi \qquad (1)$$

where θ is the angle measured as shown in Fig. 1. Since the magnetic field on the plasma axis in the central cell is about 4.7 tesla and is in the z direction, the magnetization of the HT-9 reaches its saturation value M_s and is in the direction of the field. The value of M_s is a varying function of the temperature and is zero at the Curie temperature of HT-9 which is about 700°C. To a very good approximation in the temperature range between 330°C - 500°C the magnetization in the left half of the blanket can be written as

$$\overline{M} = M_s\hat{z} = (A - B\theta)\hat{z} \qquad (2)$$

where the constants A and B can be determined by knowing the value of M_s at the inlet and the outlet temperatures, and $\hat{z}$ is a unit vector in the z direction.

Magnetic Field Due to Magnetized Structure. If one knows the distribution of the magnetization in the magnetized structure, one can estimate the field due to such structures (outside it) by using either the corresponding distributions of the magnetic pole densities given by:[1]

$$\text{surface pole density} = (\overline{n} \cdot \overline{M}), \text{ and} \qquad (3)$$
$$\text{volume pole density} = -\overline{\nabla} \cdot \overline{M} \qquad (4)$$

or by the corresponding distribution of the Amperian current densities given by

$$\text{surface current density} = (-\overline{n} \times \overline{M}), \text{ and} \qquad (5)$$
$$\text{volume current density} = (\overline{\nabla} \times \overline{M})\ . \qquad (6)$$

Consider first the case where no temperature variation exists, i.e., the magnetization is uniform and constant ($\overline{M} = M_s \hat{z}$). In this case both $\overline{\nabla} \cdot \overline{M}$ and $\overline{\nabla} \times \overline{M}$ vanish. Thus, we could simulate the effect of the magnetized blanket by either a surface pole density ($\overline{n} \cdot \overline{M}$), which will have values only at the end faces of the blanket, or by surface current densities ($-\overline{n} \times \overline{M}$) which will have equal but opposite values on the outer and the inner surfaces of the blanket. It appears directly from using any of these two models that the field due to the magnetized structure will be only at the far ends of the blanket.

Now consider the case in which the magnetization obeys Eq. 2. The volume current density exists and has a value in the radial direction only, i.e.,

$$\overline{\nabla} \times \overline{M} = \overline{\nabla} \times (\overline{M}_s z) = \left(\frac{1}{r} \frac{dM_s}{d\theta}\right) \hat{r} = -B/r \, \hat{r} \, , \qquad (7)$$

using Eq. (2). If this value is multiplied by an infinitesmal volume $dv = rd\theta drdz$, the result will be $-B\hat{r}\, drd\theta dz$ and this is equal and opposite to the difference between the surface current at θ which is $M_s(\theta)\hat{r}\, drdz$ and the surface current at $\theta + d\theta$ which is $-(M_s + (dM_s/d\theta) \cdot d\theta)\hat{r}\, drdz$, i.e., $-(dM_s/d\theta)d\theta\, \hat{r}\, drdz$. Thus, the volume current density cancels the net radial current which is due to the variation of the magnetization, and the effect appears only at ends of the blanket as before but in a different way. This conclusion could be reached directly using the pole model where $\overline{\nabla} \cdot \overline{M}$ is zero, but the current model shows more clearly how the temperature effects disappear at the center of the central cell.

The conclusion, based on this simple model, is that the variation of the magnetization of the ferromagnetic structure will be only at the end of the blanket. Numerical calculations showing the field at the ends of the blanket will be presented.

[1] W.F. Brown, "Magnetostatic Principles in Ferromagnetism," North-Holland Publ. Co., 1962.

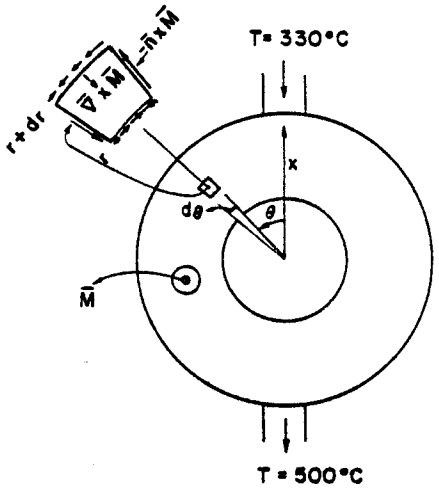

Fig. 1. Schematic cross section for the blanket. The arrows in the infinitesimal area show the directions of the surface current densities ($-\overline{n} \times \overline{M}$) at each side, and the direction of the volume current density ($\overline{\nabla} \times \overline{M}$).

ENGINEERING DESIGN OF THE QUASI-OPTICAL ECRH INJECTION SYSTEM FOR THE MIRROR ADVANCED REACTOR (MARS)*

L. John Perkins
Fusion Engineering Program
Nuclear Engineering Dept.
University of Wisconsin
Madison, WI 53706

Steven A. Freije
TRW Energy Development Group
One Space Park
Redondo Beach, CA 90278

A complete high-power steady-state ECRH injection system has been designed for the MARS tandem mirror reactor and is presently being optimized for overall economic performance. The system consists of a Graetz bridge AC-DC 90 MW power supply, 1 MW gyrotrons with depressed collector operation and a novel quasi-optical launching system for the combination and transmission of the ECRH power from the individual gyrotrons to the plasma.

The Mirror Advanced Reactor Study[1] (MARS) is a major two year conceptual design study of a commercial tandem mirror reactor. It is currently being conducted by Lawrence Livermore National Laboratory in conjunction with the University of Wisconsin and TRW as the prime industrial contractor. Electron cyclotron resonance heating (ECRH) is an essential requirement in MARS for the maintenance of the potential peaks and thermal barriers in each of the end plug yin-yangs of the device. In the current baseline design, 53 MW of ECRH power at 64 GHz produces a collisionless mirror-trapped hot electron population at the minimum-B point (2.3 tesla) and is required for the formation of the thermal barriers. Similarly, a further 2 MW of ECRH power at 96 GHz contributes to the maintenance of the confining electrostatic potential peaks at the 3.4 tesla point. ECRH systems on current and projected near-term experimental devices exhibit powers of only ~ 80-200 kW at 28, 35 or 50 GHz and, furthermore, are not steady state. These systems typically comprise charged capacitative pulsed power supplies, gyrotron units of up

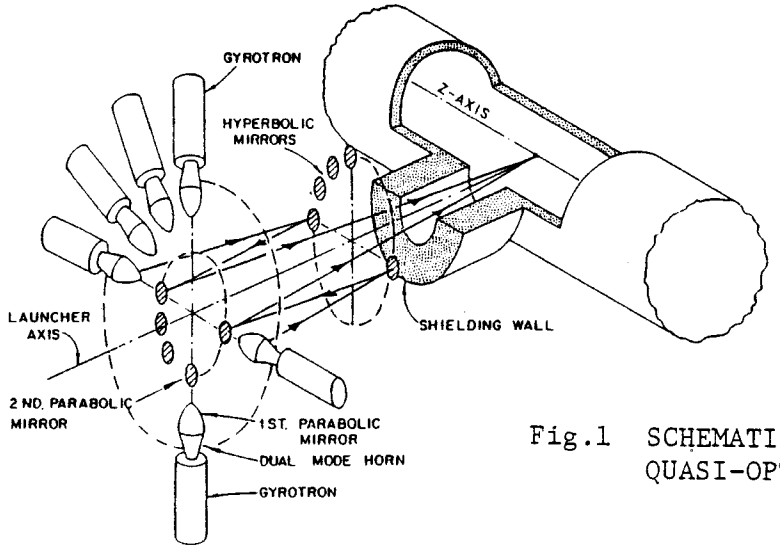

Fig.1 SCHEMATIC OF THE MARS ECRH QUASI-OPTICAL LAUNCHING SYSTEM

to only 200 kW and metallic waveguide transmission systems. However, such systems become inefficient, expensive and impracticable when scaled to the reactor requirements of MARS which call for CW-mode ECRH power in the range 50-60 MW. Accordingly, a complete steady state 55 MW ECRH injection system has been configured for this reactor.

Fig. 1 shows schematically one of the 64 GHz quasi-optical launchers for MARS. The ECRH field is launched in a beam-mode (rather than the wave-mode of conventional metallic waveguides) by an array of dual-mode horns fed by gyrotron sources after appropriate mode conversion. Propagation proceeds via the lowest loss TEM_{oo} mode with a radial Gaussian distribution of the electric field. The beam mode is transported to the plasma via a phased array of hyperbolic and parabolic mirrors arranged in an offset Cassegrain configuration.

The quasi-optical launching system offers several distinct advantages over the more conventional overmoded waveguide systems and affords a low loss (~ 11%) combination of gyrotron sources to multi-MW levels with minimal space requirements. In particular, since the ECRH propagates in a Gaussian beam-mode rather than a wave-mode, power density constraints are alleviated and the system can be operated in vacuum without the need for ceramic windows.

The 1 MW gyrotron with depressed collector was selected as the base-case microwave source for this system and has specified operating characteristics of 150 kV at 8.5 A, a collector voltage of -40 kV and an estimated net efficiency of ~ 80%. A Graetz bridge AC-DC convertor supplies ~ 600 A DC at 150 kV to the gyrotron cathodes and was chosen on the grounds of both economics and reliability. The launcher in Fig. 1 contains a total of 17 gyrotrons including two for reducing purposes and has a design power of 13.25 MW. Two such launchers are therefore required at each end of the machine giving a total ECRH injected power of 55 MW at 64 GHz. Some characteristic dimensions of this launcher are a total length of ~ 20 m with hyperbolic and parabolic mirror diameters of 0.38 and 0.54 m, respectively.

In conclusion, the quasi-optical system provides a very attractive method of launching ECRH into the Mirror Advanced Reactor and avoids many of the problems of conventional metallic waveguide systems. In addition, a comparative trade study of the capital cost and recirculating power requirements for a number of ECRH configurations for MARS has concluded that, given the current and projected development programs, the Graetz bridge power supply together with the 1 MW gyrotron with depressed collector will provide a near optimum system in terms of economics, reliability and performance.

[1]"Mirror Advanced Reactor Study (MARS) Interim Design Report", UCRL-53333, Lawrence Livermore National Laboratory (1982).

*Funding for this work was provided by the U.S. Department of Energy.

MARS HEATING SYSTEMS*

S.A. Freije, D.J. Goebel
Energy Development Group, TRW, Inc., Redondo Beach, CA

L.John Perkins
Nuclear Engineering Dept., Univ. of Wisc., Madison, WI

The Mirror Advanced Reactor Study (MARS) addresses a commercial tandem mirror reactor. The reactor is a linear magnetic fusion device with the axicell configuration. MARS utilizes electrostatic plugs to confine a steady-state fusion plasma in the solenoidal central cell.

The endplugs, which contain the thermal and potential barriers, require a number of heating systems to produce the necessary potential and density profiles, thus ensuring stability, confinement, and overall desirable operating characteristics. The heating systems have a large impact on both capital cost and recirculating power requirements. They include: 1&2) a high energy neutral beam system and an electron cyclotron resonance (ECRH) system to maintain the potential barrier, 3) a moderate energy neutral beam to charge exchange pump the transition region, 4) another ECRH system to maintain a mirror trapped electron distribution in the thermal barrier, and 5) an ion cyclotron resonance heating (ICRH) system to heat ions in the high field mirror region, the axicell region, thus producing a potential bump to control the passing ion density. The basic characteristics of each of these systems are presented as well as their integration in the end plug geometry.

The two ECRH systems deliver 55MW of power to the plasma. Theoretical studies are being performed to determine the frequencies for optimum wave penetration and absorption; a beta correction and the relativistic shift may force a decrease in the injected frequencies from the 64GHz and 95GHz vacuum values. An extensive trade study analysis has been performed to determine the most efficient, economical ECRH system within the technology development constraints of MARS. The basic system consists of a Graetz bridge power supply, a MW gyrotron with a depressed collector, and a quasi-optical launcher and transmission system. The quasi-optical system is an offset Cassegrain system with a dual-mode conical horn/paraboloidal reflector as a launcher.

Power balance calculations indicate that 40MW of ICRH power must be absorbed by the axicell ions in order to maintain the mirror trapped distribution. An 85% ion absorption efficiency requires 47MW of delivered power. The vacuum field at the axicell midplane is 18T; as beta increases, the resonance surface moves 20cm off midplane. The second harmonic frequency at this field for tritium is 182.4MHz. When magnets, shields, structure, coolant feeds, etc. are taken into account, the ICRH launcher must fit into a very restricted space. Because of the geometry constraints of the region, an antenna launcher is considered.

The system consists of a multi-stage amplifier chain with associated power supplies, power splitters and combiners, a coaxial transmission line with multi-stub tuning, and a launcher which is a short-circuited section of stripline electrostatically shielded by an array of metal strips.

The MARS reactor baseline requires that 1480A of neutral beam current at 94keV be injected 30° with respect to the plasma axis for charge exchange pumping. Due to the high injected power of this system, 140MW, the beam lines must be as efficient as possible and yet represent reasonable technology advances in the MARS time frame. The partial energy species (from the dissociation of molecular ions from the positive ion sources) that are injected, become trapped and must be removed by additional pumping current, or they must be separated and collected prior to injection into the plasma. For these two reasons, high efficiency and species mix negative ion based systems have also been considered. The selection of the pump beam system will be made in the second half of the program.

Positive ion pump beamlines contain four sources, each with an extraction area of 15 x 70cm^2 and average current density of 120mA/cm^2. The source configuration for continuous plasma production and confinement has not been developed, but will probably contain magnetic multipole confinement and either hollow cathode or rf plasma generation. The accelerator utilizes multiple cooled rails with a 40% transparency and ½° x 1° divergence. An LBL filter system to separate the molecular species is a set of thin rows of magnets in the decel region of the grids, shielded by accelerator electrodes, and is currently under development. The unneutralized portion of the beam is bent and directly recovered after passing through a closely coupled gas neutralizer.

The sources for a negative ion pump beamline are cesiated surfaces which convert positive ions formed by an rf plasma generator in a magnetic multipole bucket containment geometry into negative ions. It is assumed to have a 50mA/cm^2 average current density with multiple sources per beamline. The accelerator will be either the LBL single slot configuration or the conventional multi-rail type with the same optics as the positive beam accelerator. The neutralizer utilizes a laser resonator photo-detachment cell with a 95% stripping efficiency.

The sloshing ion beamlines must deliver 39.2A at 475keV and injected 90° with respect to the plasma axis. The low efficiency of a positive ion system at this energy and the low current requirement leads to the selection of a negative ion system. The sources are similar to those described for the negative ion pump beam, but will form circular beamlets for the accelerator. The plasma generator operates continuously with an electrical efficiency of 5kW per ampere of negative ions and 30% gas utilization efficiency. The DC-ESQ accelerator is basically a DC-megalac where the acceleration occurs between focusing stages over an extended accelerator length. The ions from the source must be pre-accelerated by a standard DC multiple grid accelerator to 50-100keV before being injected into the quad system. As for the negative ion pump beam, a laser photo-detachment neutralizer is used.

These five heating systems must be integrated with all the other endcell systems. The endcell configuration and layout are presented.

*Work supported by Lawrence Livermore National Laboratory contract number 5299101

DESIGN OPTIMIZATION OF THE MARS LiPb BLANKET*

L. John Perkins
Fusion Engineering Program, Nuclear Engineering Department
University of Wisconsin, Madison, Wisconsin 53706

The Mirror Advanced Reactor Study[1] (MARS) is a major conceptual design study of a commercial tandem mirror reactor currently being conducted by Lawrence Livermore National Laboratory in association with the University of Wisconsin and with TRW as the prime industrial contractor. One of the objectives of this study was the design of a LiPb blanket, comprising a flowing liquid $Li_{17}Pb_{83}$ breeder/coolant contained in HT-9 ferritic steel structure. The blanket was required to be simple in concept, easy to fabricate and provide for convenient maintenance. However, given these initial constraints, the following important question was posed: For a fixed neutron power from the fusion plasma, how should both the structural and neutronic designs proceed in order for the economic performance of the blanket to be optimized? Accordingly, a self-consistent design optimization procedure was established. Ths procedure is not necessarily specific to MARS and has general applicability to fusion reactor blanket design optmization.

In the initial stages of blanket design, it is necessary to consider a complex set of issues and requirements which are often conflicting. For example: what value of tritium breeding ratio is required? What is the maximum neutron energy multiplication factor (M) attainable for this blanket concept? Should we design a thick blanket in order to maximize M or should we design a thin blanket in an attempt to minimize overall central cell costs (including radiation shield and magnets, etc.?) Would a thin blanket and corresponding thick radiation shield be more expensive than a thick blanket with a corresponding thin shield? Would a thin blanket result in a larger energy deposition in the reflector/shield with an associated economic penalty in thermal cycle efficiency? How do superconducting magnet radiation limits influence the economics of the blanket, reflector and shield, etc.?

In examining optimization questions such as those above, it was determined that all constraints and requirements must be formally integrated into a systematic design optimization procedure such that progress in the LiPb blanket design could be assessed in terms of improved economic performance. This design procedure is necessarily iterative and requires the minimization of an economic figure of merit F for the overall reactor system. The procedure can be summarized as follows:

1. Establish a self consistent economic figure of merit F for overall system optimization (see below).

2. Specify the required tritium breeding ratio (TBR) for the blanket system.

3. Establish a blanket and reflector point design by specifying dimensions, volume fractions of LiPb and HT-9 structure, ^{6}Li enrichment, etc. Perform neutronics analyses on this design to obtain the blanket multiplication factor (M) and fractional energy deposition in the

reflector for the required constant TBR.

4. Determine gross thermal efficiency η and LiPb pumping power for the thermal hydraulic (heat transfer) system.

5. Determine neutronic design constraints for central cell magnets and required external radioactivity conditions at shutdown. Design blanket shielding so that all conditions are satisfied and, thereby, determine minimum inside radius of magnet winding pack.

6. Determine magnet winding pack dimension and magnet center-center spacing so that the desired magnitude and ripple of the central cell magnetic field are obtained. Ensure magnet configuration is consistent with blanket maintenance requirements.

7. Cost all reactor items which depend on either the blanket multiplication factor M or thermal cycle efficiency η (e.g., blanket, reflector, shield, magnets, thermal hydraulic system, turbine and electrical plant equipment, etc.).

8. Compute the economic figure of merit parameter F.

9. Iterate the above procedure from step 3 and, by variation of the point blanket/reflector design, minimize the figure of merit parameter F.

Establishment of this self-consistent figure of merit parameter F required a detailed sensitivity analysis for the system. Through this it was determined that F must explicitly incorporate the overall capital cost of the reactor (both blanket-dependent and non-blanket-dependent items) normalized by the net electrical power (MWe) of the system (i.e., total MWe produced from the blanket and from the direct convertor minus the recirculating power requirements).

Application of the iterative optimization procedure resulted in a blanket of small radial thickness of ~ 38 cm containing highly enriched (90%) ^{6}Li. Small radial dimensions enabled other central cell dimensions and capital costs (e.g., for reflector, shield, magnets, etc.) to also be kept small. At the same time, optimization of the LiPb/structure volume fractions and corresponding radial zoning enabled the attainment of a large blanket multiplication factor M of ~ 1.4, for a constant tritium breeding ratio of ~ 1.1. The resulting minimization of the figure of merit parameter F yielded a LiPb blanket design for the MARS tandem mirror reactor, exhibiting optimum economic performance. A detailed description of this final optimized design may be found elsewhere in these proceedings.

*Funding for this work was provided by the U.S. Department of Energy.

[1]"Mirror Advanced Reactor Study (MARS) Interim Design Report", UCRL-53333, Lawrence Livermore National Laboratory (1982).

THERMAL AND MECHANICAL DESIGN OF A DOUBLE-WALLED STEAM GENERATOR

D.C. Schluderberg
Babcock and Wilcox Company
Lynchburg, Virginia

J.H. Huang
L. Pong
D.K. Sze
University of Wisconsin
Dept. of Nuclear Engineering
Madison, Wisconsin 53706

Heat exchange equipment for the MARS power cycle must fulfill exacting requirements, while at the same time retain design features acceptable to the utility industry.

The normal difficult design requirements of liquid metal to water heat exchangers is further complicated by the following:

- The component must provide a tritium diffusion barrier between blanket coolant and steam cycle.
- The component design must permit practical inspection and maintenance procedures in spite of radiation levels produced by activated corrosion products present in the blanket coolant.

The design described in Figs. 1 and 2 was created to meet the above difficult requirements. It provides the following features:

- Provision of an adequate tritium diffusion barrier.
- Detection of potential tube defects that could lead to metal/water reactions.
- Avoidance of size limitation problems typical of double walled heat exchangers.
- Detection, location and repair of leaks by conventional methods (eddy current).
- More compact construction.
- More conventional, less difficult component assembly.

The space between inner and outer shells and between inner and outer walls of each tube assembly is filled with helium containing oxygen at a partial pressure of one torr. A pumping system (not shown) is used to circulate this gas longitudinally through each tube wall gap as a sweep (or monitor) gas to detect water vapor.

The hemispherical heads shown in Fig. 1 are similar in configuration to those used for "once through" PWR steam generators. Thus, the tube inspection repair equipment developed for this equipment is applicable to the design shown in the above figure.

This equipment has been used satisfactorily to perform inspection and

maintenance work in radiation levels up to about 15 rem at the hemispherical head tube face.

To cope with higher radiation levels, the manways can be replaced by full opening closures, which in turn will permit use of rotating plugs and other equipment developed in the past for hot maintenance.

The effect of activated corrosion product radiation upon inspection and maintenance tends to be minimized by the following:

- Vertical (instead of horizontal) tube sheet faces. This reduces collection of corrosion particles on these surfaces.
- Inner and outer tube sheets with a space between. This attenuates streaming of gamma rays through tube ID's.
- Corrosion products will tend to collect at the top of the inner shell. Radiation from this location will not be in line with tube sheet holes.

The tritium isolation is provided by the air gap and the oxide coatings facing the air gap and facing the steam side. A finite difference computer code is developed to perform the mass diffusion calculations. A diffusion barrier factor of 10^5 is obtainable comparing to a single walled steam generator with no oxide coating. The tritium leakage rate is < 10 curies/day.

The heat transfer across the gap and its impact on thermal efficiency on the power cycle is also calculated. The steam generator area is 25% larger than a single-walled steam generator.

Acknowledgement

This work is partially supported by DOE. The preparation of the manuscript by Gail Herrington is much appreciated.

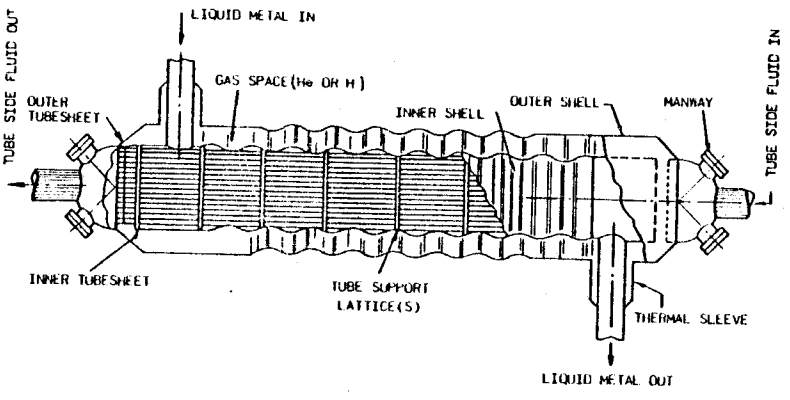

Figure 1 Double-walled steam generator general arrangement

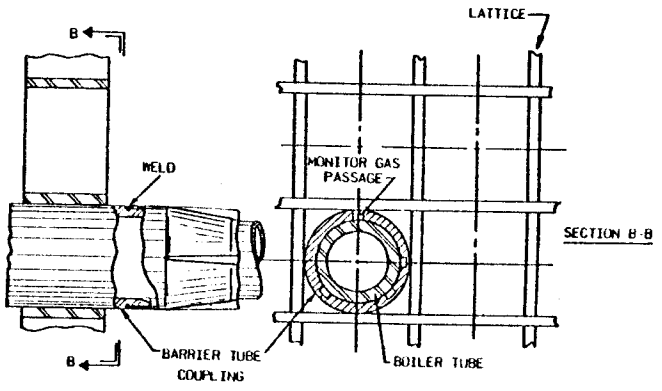

Figure 2 Double-walled steam generator tube support detail

EMERGENCY COOLING OF THE MARS LiPb BLANKET

D.K. Sze and A. White
University of Wisconsin
Nuclear Engineering Department
Madison, Wisconsin 53706

The thermal response and cooling requirement of the MARS LiPb blanket due to the afterheat, loss of coolant and loss of flow are reported here. The effects of the accident, if proper cooling is not available, are also discussed. The most critical accident that may occur is the loss of coolant while the plasma is still on. The first wall will suffer permanent damage in ten seconds, and it will melt in ~ 35 seconds.

The afterheat is calculated by ANISN and DKR codes. A forward 25 neutron 21 gamma group ANISN run was done in order to obtain the steady state flux throughout the blanket and shield region. This output was then fed into the DKR program. This produced a delayed gamma source spectrum and also gave the total beta heat produced in each zone. The gamma source was then fed back into the ANISN program and a forward 21 group gamma transport problem was run. In this calculation, activation cross sections were used to determine the heat deposition in each region, and in each material. This calculation was performed for each region after shutdown and was performed for both the case of the LiPb remaining in the reactor and the case of LiPb drained from the blanket. In all, a total of 12 ANISN runs were made. Finally, the beta heat from the DKR and the gamma heat from ANISN were summed to give the total afterheat in each zone. The results of these calculations are given in Fig. 1.

The very high afterheat in the reflector at shutdown should be noticed. This is due to the ^{56}Mn in Fe-1422. The half life of ^{56}Mn is 2.6 hrs and, therefore, the afterheat of the reflector decays rapidly in the first day. After one day, the reflector can be used as the heat sink for radiation cooling of the blanket. The blanket needs active cooling for the first day. It can be cooled effectively after that and maximum temperatures due to afterheat may reach 390°C.

The temperature responses of the first wall due to loss of flow and loss of coolant accident are calculated and shown in Fig. 2. The rate of the first wall temperature rises are very similar in the two cases. The reason for this unexpected result is due to the much higher volumetric heat capacity for steel (ρ_{cp} = 3.6 j/cm^3-°C) than for the $Li_{17}Pb_{83}$ (ρ_{cp} = 1.5 J/cm^3-°C). Therefore, in the loss of flow accident case, the temperature rise of the $Li_{17}Pb_{83}$ is actually faster than the structure although the volumetric heating rate is less. The coolant will heat up the first wall and, consequently, the first wall is heated up faster than the loss of coolant accident case. As time reaches ~ 20 seconds, the $Li_{17}Pb_{83}$ further away from the first wall (with a consequent much lower volumetric heating), starts to cool the first wall by conduction. This explains the crossover point of the two temperature response curves.

If loss of flow or loss of coolant occurs, the blanket will suffer permanent damage if the plasma is on for ten seconds. If the plasma is not stopped in ~ 35 seconds, the first wall will melt.

In a liquid metal flow system, a surge tank is always provided to maintain a free surface. The $Li_{17}Pb_{83}$ in the surge tank can be used as the emergency coolant by using gravitational force to pump. A coolant velocity of 7 cm/sec can be reached by using the gravitational head. The temperature response of the first wall is shown in Fig. 3 and will reach a maximum of 800°C in ~ 30 sec. The coolant flow rate required is 5 m^3/sec for the entire reactor. The total emergency cooling time provided has to be optimized between surge tank cost and accident detection time.

Acknowledgement

This work is supported by DOE. The work by Gail Herrington in preparing the manuscript is much appreciated.

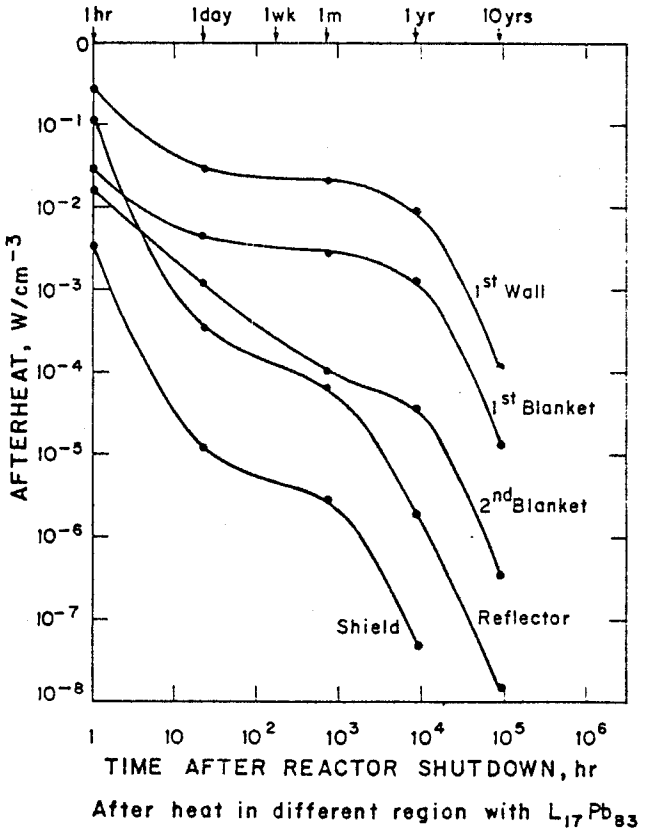

Figure 1

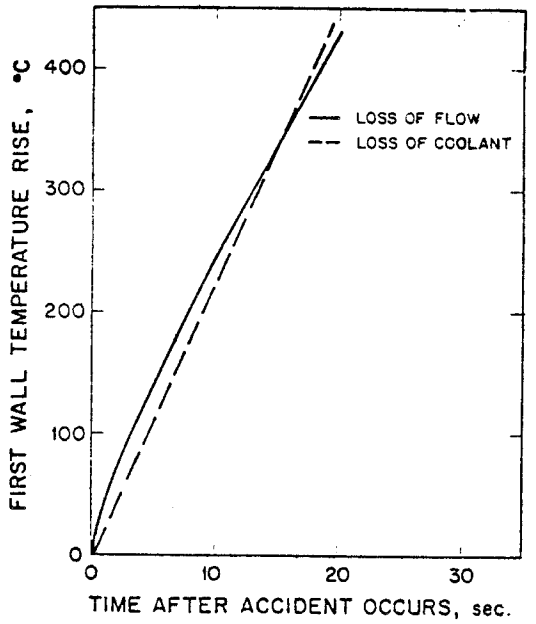

Figure 2 Temperature response of the first wall

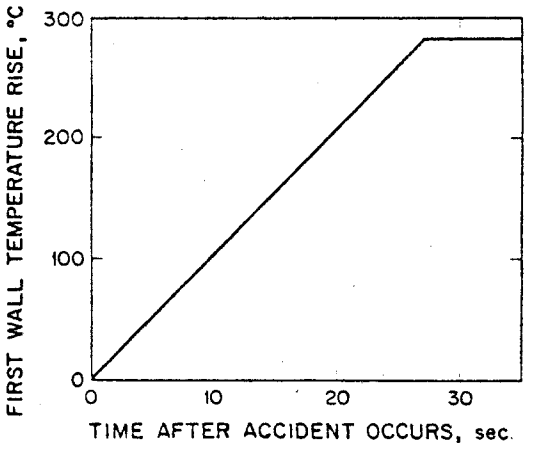

Figure 3 Temperature response of the first wall with gravitational coolant flow

MARS AXICELL RADIATION DAMAGE AND SHIELDING ANALYSIS

Laila El-Guebaly, L. John Perkins, and C.W. Maynard
Nuclear Engineering Department, University of Wisconsin

The MARS tandem mirror reactor[1] employs a high field axicell to mirror-confine plasma particles without radial drift. This region presents important magnet and shield problems to the designers. The field on axis at the highest point is 24 tesla. Production of this large magnetic field requires the use of a hybrid solenoid where outer superconducting (S/C) coils produce ~ 14 tesla of the required axial field, while inner normal conducting insert coils supply the balance. Figure 1 illustrates the geometric configuration of the MARS axicell coils. The two inner normal conducting coils are positioned with their inner bore behind the first wall with no intervening shielding and are located coaxially with respect to the outer superconducting coils. Shielding is placed between the normal and S/C coils and ensures the operational integrity of the latter.

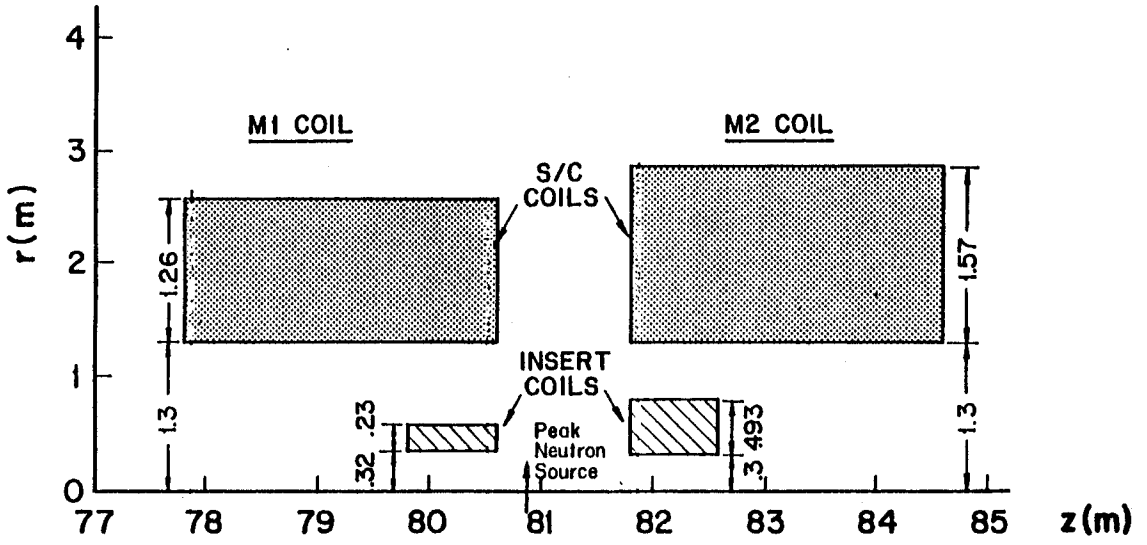

Fig. 1. Geometrical configuration of MARS axicell coils.

The radiation transport problem is modeled as an infinite cylinder and discrete ordinates calculations are carried out using ONEDANT to investigate the various responses of interest. In the normal coils there is concern with both electrical and mechanical degradation of the ceramic insulation and the electrical resistivity of the copper conductor due primarily to transmutations. An additional potential problem is radiolytic decomposition of the water coolant leading to corrosion product formation. Problems of concern in the S/C coils are the dose to the polyimide insulation, heating in the S/C magnet, and dpa to the copper stabilizer of the conductor. The final problem concerns the difficulties of shielding the S/C magnets in the presence of penetrations since clearances are always tight between coils.

The wall loading in the axicell is over 4 MW/m^2. This results in a peak fluence of neutrons above 0.1 MeV in the Spinel used as insulator for the normal coil of 3.5×10^{22} $n/cm^2/FPY$. Mechanical integrity of the insulator manifests itself in this case by swelling and the amount of swelling that can be tolerated is a design parameter which must be set. Transmutations in the copper winding produce impurities which increase the resistivity and in turn increase the ohmic heat to be removed by the cooling system. The limiting value is again a design parameter which must be set but it will limit the useful coil life. These two limits combine to insure the necessity of replacement of the normal coils on the order of two years unless shielding is introduced in front of the coils.

In order to keep the S/C coils as small as possible the shield is optimized for a 75 cm shield thickness using the three responses mentioned above. The result was a 73 cm tungsten region backed by a 2 cm B_4C region. This actually provided somewhat more shielding than the design goals and to make the shield somewhat less expensive without redesign of the magnets we replaced the last 14 cm of tungsten with Fe-1422 stainless steel.

In order to assess the shielding problem posed by the neutral beam injection (NBI) duct, a three-dimensional radiation transport model was implemented using the Monte Carlo code MCNP. The NBI duct is located midway between the two coils. The duct injection angle is 90 degrees and the duct opening is 32.5 by 48 cm and the first wall radius is at 30 cm at the location of the duct. The S/C winding pack is located at 130 cm from the plasma centerline, the equivalent thickness of steel provided by the magnet case and the cryostat is 5.8 cm which left 33.75 cm available for the shield between the duct wall and the S/C magnet. The calculational results indicate a peak dpa in the copper stabilizer of 3.6×10^{-4} dpa/FPY. In order to limit anneals of the S/C windings a limit of 1.9×10^{-4} dpa after 5 FPY has been adopted. Thus the shield is inadequate on this basis. An estimate was made as to the required shield leading to a need for a 46 cm shield. This led to the abandonment of the use of neutral beam injection in this region in later versions of MARS.

One major conclusion here is that it is possible with proper design to place normal coils immediately behind the first wall provided one is prepared to change out the coil in about two operating years. In addition it should be noted that considerable care should be taken to provide adequate clearance between coils if NBI's are to be used in high neutron source zones.

[1]"Mirror Advanced Reactor Study (MARS) Interim Report," UCRL-53333, Lawrence Livermore National Laboratory (1982).

This work was funded by the United States Department of Energy.

MECHANICAL AND THERMAL DESIGN ASPECTS OF THE BLANKET, AND MAINTENANCE CONSIDERATIONS OF THE CENTRAL CELL IN MARS

Y.T. Li, D.K. Sze and I.N. Sviatoslavsky
Fusion Engineering Program
Nuclear Engineering Department
University of Wisconsin

MARS is a conceptual design of a tandem mirror fusion power reactor. A primary objective of the blanket design is to take maximum advantage of the linear geometry of the tandem mirror in order to achieve a straightforward maintenance approach which can be performed rapidly by remote control. This paper briefy describes the mechanical and thermal blanket design aspects, then addresses the maintenance concept of the central cell.

Figure 1 shows a cross section of the central cell which is a linear cylinder ~ 150 m long in which most of the energy is produced. In this design the blanket structure is HT-9 and the breeding material is $Li_{17}Pb_{83}$. The breeding material is fed at 330°C through a supply header, is distributed axially in the upper manifold, then flows through tubular and rectangular section beams to the lower manifold, finally exiting at 500°C through a discharge header. The blanket is divided axially into modules which have individual supply and discharge headers. A gap is provided between the blanket modules and the reflector to allow axial translation of the modules within the central cell. There are no seals between adjacent blanket modules, instead a vacuum barrier is provided at the reflector boundary along the whole central cell. The modules are supported on rails attached to the reflector with the load path going through the shield to the floor supports.

The motion of a liquid metal perpendicular to a strong magnetic field is characterized by laminar flow with a constant velocity profile and a very thin boundary layer. Heat transfer in such a system is dominated by conduction. The temperature distribution in the blanket tubes can be calculated by solving a set of finite difference equations. For this design, the maximum structural temperature is 550°C.

The MHD pressure drop through each blanket section is the sum of the Hartman and the end of the loop pressure drops. This pressure drop is determined to be 1.32 MPa, which corresponds to a pumping power of 40 MW for the whole central cell, if a 50% efficiency is assumed. The maximum pressure in the blanket is only 0.9 MPa.

The maintenance philosophy is to achieve a high reactor availability by minimizing the downtime due to routine blanket changeout. Because maintenance will be performed remotely, this concept avoids welding or cutting of headers, reflector or shield segments and requires no axial translation of central cell coils.

Access to the blanket is provided through twelve so-called service stations as shown in Fig. 2. These stations are equipped with a

removable supply header, vacuum lid and an upper reflector/shield segment. Each station is capable of servicing seven blanket modules, the one immediately below and three on either side. Once the supply and discharge headers are disconnected, blanket modules are translated axially to the service station, then lifted out vertically by an overhead crane. The axial length of the blanket modules was determined by taking into account the space between central cell coils and the size and location of the breeding material headers which go through this space. Advantage is taken of the excellent soldering capability of $Li_{17}Pb_{83}$ to design truly simple remotely maintainable header connections.

Unexpected maintenance of other central cell components such as the coils, shield and reflector segments is also addressed.

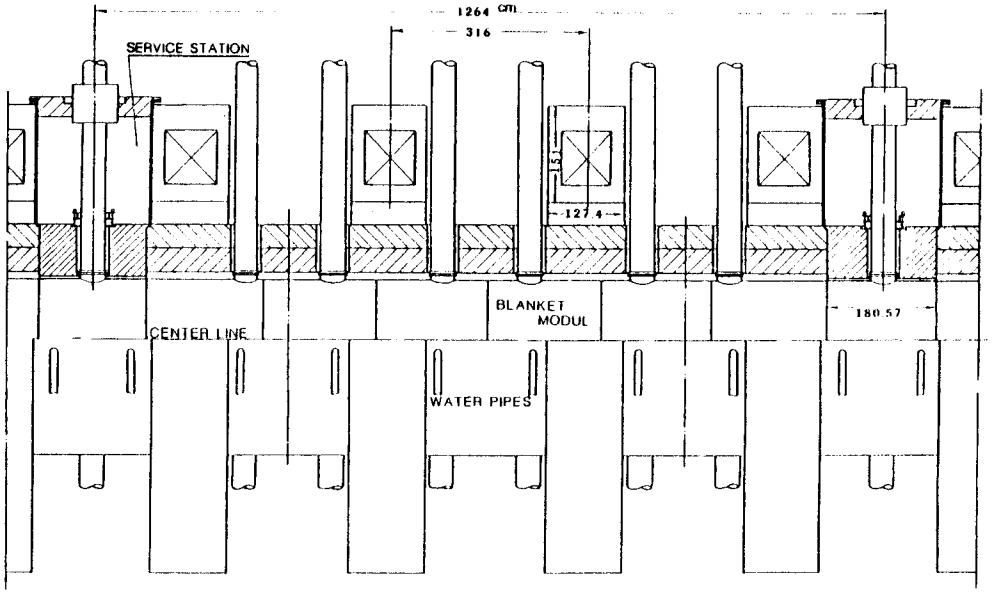

Fig.2 CENTRAL CELL ASSEMBLY

84 BLANKETS
12 SERVICING STATIONS
TOTAL LENGTH OF C.C. 151.68m

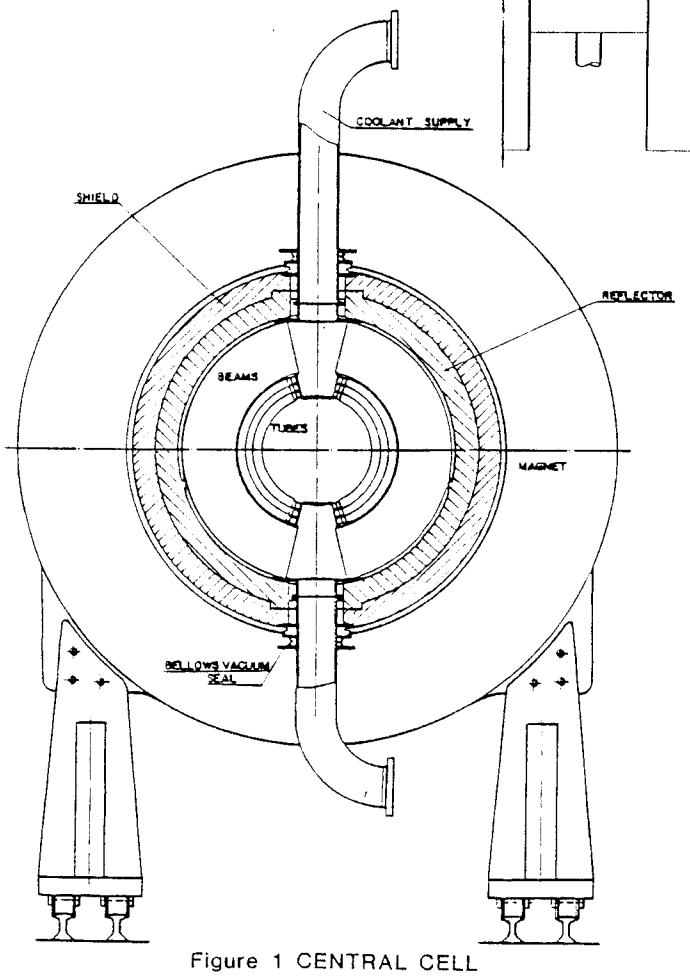

Figure 1 CENTRAL CELL

NEUTRONICS ANALYSIS FOR THE MARS Li-Pb BLANKET AND SHIELD

J.H. Huang and M.E. Sawan
University of Wisconsin
Department of Nuclear Engineering
Madison, Wisconsin 53706

The MARS (Mirror Advanced Reactor Study) fusion power reactor design employs a long central cell consisting of a number of blanket modules. Neutronics analysis has been performed to determine the blanket design which yields the largest energy multiplication (M) with adequate tritium breeding ratio (T). This will have an impact on reducing the overall cost of produced electricity. This analysis is aimed also at designing a shield which provides adequate radiation protection for the superconducting magnets. The Li-Pb blanket of MARS uses $Li_{17}Pb_{83}$ as the breeder and coolant and the ferritic steel HT-9 for structure. The blanket consists of a front tube zone and a back zone of rectangular beams which provide the structural support. The blanket is followed by a water cooled stainless steel reflector. The energy deposited in the blanket and reflector is recovered and represents the reactor's thermal power.

The continuous energy Monte Carlo code MCNP was used with cross secton data based on the ENDF/B-V evaluation to determine the appropriate composition and thickness of the blanket and reflector. The continuous energy treatment of MCNP was used to eliminate energy group structure effects. Our results show that both T and M are sensitive to the group structure in a Li-Pb system. Furthermore, data based on ENDF/B-IV tend to overestimate T and underestimate M when compared to ENDF/B-V data. 4,000 histories were used in the calculations resulting in statistical uncertainties less than 1% for the quantities of interest.

The results show that neutron multiplication through the Pb(n,2n) reaction saturates to a value of ~ 1.75 at a blanket thickness of ~ 30 cm. This implies that, from the point of view of neutron multiplication, the lead in the back region of the blanket is ineffective. Hence, a thin blanket design, in which the lithium is enriched to 90% ^6Li, was considered and compared to a thick blanket design in which natural Li is used. A saving of 49 cm (38.2 versus 87.2 cm) in blanket thickness is achieved for the same T. This results in reducing the central cell cost because of the associated smaller magnet size. Furthermore, the blanket has less weight and can be easily changed out. However, a smaller M is obtained from the thin blanket when HT-9 is used as a reflector. Several attempts have been made to enhance the energy multiplication while preserving the advantages associated with the thin blanket design.

Increasing the Li-Pb content in the beam zone of the blanket was found to increase M. A beam zone consisting of 85 v/o $Li_{17}Pb_{83}$ and 15 v/o HT-9 has been chosen. Further enhancement of M can be achieved by appropriate choice of reflector material. For a thin blanket, a relatively large fraction of energy is deposited in the reflector and the overall energy multiplication is sensitive to the choice of reflector material and thickness. Materials considered in this analysis include HT-9, 316-SS, graphite and Fe-1422. Fe-1422 was found to yield the largest M, primari-

ly due to the large gamma production in Mn. Increasing the reflector thickness was found to further increase M. A schematic of the MARS Li-Pb blanket, shield and magnet is given in Fig. 1. This blanket design results in a tritium breeding ratio of 1.13 and an overall energy multiplication of 1.39 which exceeds that obtained in the thick blanket design.

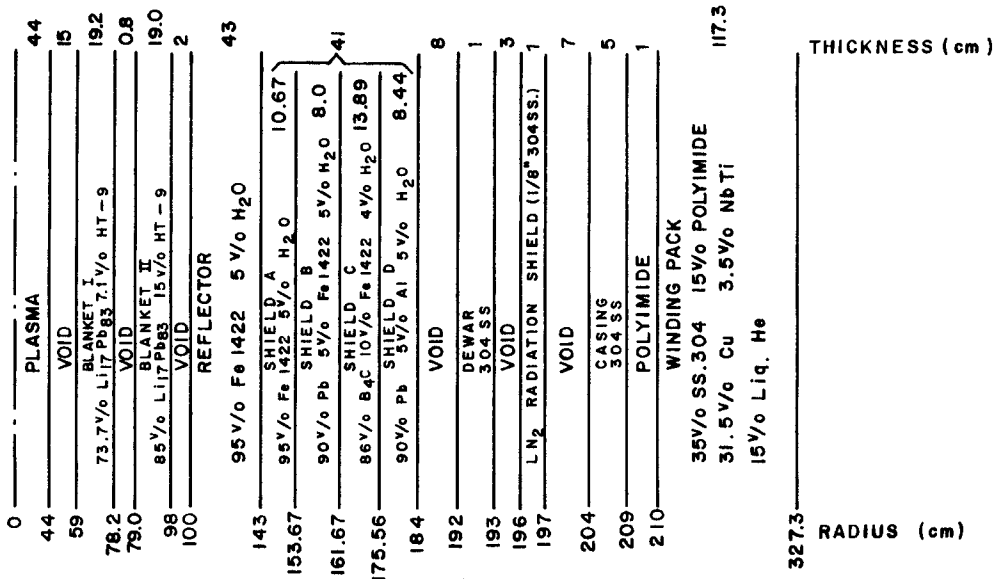

Fig. 1 Schematic of Blanket, Shield and Magnet

The shielding requirements for the 8 tesla central cell superconducting magnets are determined by a number of radiation limits. The dpa rate in Cu should not exceed 2.2×10^{-5} dpa per full power year (FPY). This is based on a 20% increase in resistivity and a minimum period of one FPY between magnet anneals. The peak dose in the polyimide insulator should not exceed 5×10^{9} rad after an estimated reactor life of 21 FPY. The limit on the peak heat-load in the magnet was considered to be 0.06 mW/cm^3. A water cooled shield consisting of layers of Fe-1422, B_4C and Pb was considered. The shield consists of four zones as shown in Fig. 1. Al-6061 is used as structural material in zone D to reduce the activation and yield acceptable biological doses at the back of the shield after shutdown. For a wall loading of 5 MW/m^2, this shield configuration was found to satisfy all design criteria.

We conclude that the thin Li-Pb blanket design for MARS results in a larger energy multiplication, a smaller magnet size and a better overall economic figure of merit as compared to the thick blanket design. Other attractive features of this design are the ease of maintenance and the reduced activated waste. The shield design for MARS provides adequate protection for the magnets and allows for hands-on maintenance at the back of the shield after shutdown.

Funding for this work was provided by the U.S. Department of Energy.

DIVERTOR TARGET DESIGN FOR THE UWTOR-M MODULAR STELLARATOR POWER REACTOR

R. Sanders and I.N. Sviatoslavsky
University of Wisconsin
Department of Nuclear Engineering
Madison, Wisconsin 53706

Modular stellarators offer a unique opportunity for innovative divertor target designs by virtue of the discreteness of their diverted flux bundles. Well focussed flux bundles leave the separatrix at discrete locations emerging from the toroid between the coil legs and then reenter the toroid.

UWTOR-M[1] is a 4800 MWth modular stellarator power reactor with 18 twisted coils and 108 divertor slots. Each divertor slot has two cylindrical divertor targets as shown in Fig. 1. The cylinders are nominally 2.5 m long and 60 cm in diameter. The divertor targets consist of stationary actively cooled shield cores which have rotating graphite surfaces surrounding them as shown in Fig. 2. The graphite shells are supported at both ends by bearings and are driven at ~ 100 RPM. They absorb the brunt of the surface heating, while the streaming neutrons are attenuated by the shielded cores. This high grade energy is then converted at a high efficiency in the power cycle.

Finite difference methods were used in a computer code to study the heat transfer from the shells. Because of the large surface area of the targets, the average surface flux is only 31 W/cm^2. Depending on the assumed emissivity of the graphite, its surface temperature falls between 1500-1600 C. Thermal conductivity of graphite has a range of 0.015 - 2.0 W/cm C depending on the type of graphite and its directional orientation. Thus, the surface temperature fluctuation can be anywhere from 30 C to 300 C, depending on the assumptions made. Changing the rotational speed from 50-200 RPM has a marginal effect on the temperature profile. It was found that a simple graphical relationship between two dimensionless variables could predict, with reasonable accuracy, the magnitude of the surface temperature fluctuations.

The external graphite layer is separated from a metallic structural frame by carbon insulation. Most of the energy is radiated from the surface with very little conduction inwards. Because of this, the surface temperature is insensitive to the thickness of the outer graphite layer. Surface erosion due to sputtering and chemical reactions, even under the most pessimistic assumptions, does not pose a problem. Sufficient graphite thickness can be provided to last between scheduled maintenance periods of approximately three full power years.

Space for bearings and drives is provided by the discreteness of the flux bundles. It would be impossible to implement such a scheme on any other magnetic fusion concept.

References

1. B. Badger, et al., "UWTOR-M, A Conceptual Modular Stellarator Power Reactor", UWFDM-550, Fusion Engineering Program and Torsatron/Stellarator Lab., University of Wisconsin, Oct. 1982.

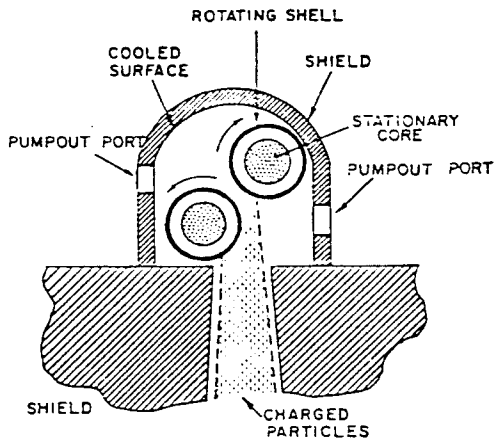

Figure 1 CROSS SECTION OF DIVERTOR TARGETS

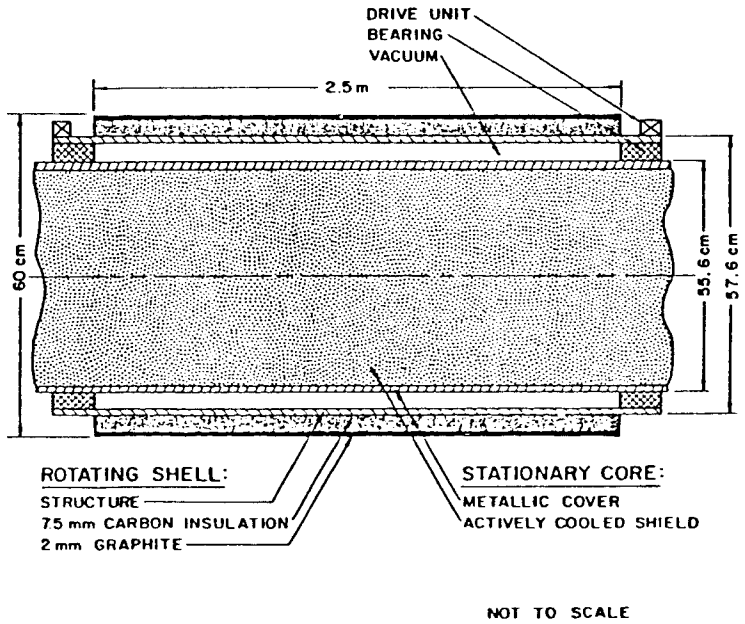

Figure 2

CROSS SECTION THROUGH LENGTH of DIVERTOR TARGET

NEUTRONICS ANALYSIS OF THE MODULAR STELLARATOR POWER REACTOR UWTOR-M

L.A. El-Guebaly
University of Wisconsin
Nuclear Engineering Department
Madison, Wisconsin 53706

Radiation streaming through penetrations in fusion reactors has significant impact on important reactor parameters such as tritium breeding ratio (BR) and energy multiplication (M). The UWTOR-M modular stellarator power reactor design utilizes large divertor penetrations for impurity control. A vertical cross section of the reactor is shown in Fig. 1. Neutronics and photonics analysis for UWTOR-M was carried out to assess radiation streaming effects on reactor performance. The breeding blanket consists of three segments with different cross-sectional areas. The radial neutron source density distribution peaks at the center of the triangular plasma zone. Some of the source neutrons will stream through the divertor slots which occupy ~ 5% of the solid angle. A significant number of lower energy secondary neutrons that have been moderated in the blanket and reflector will also stream through the slots along with some gamma photons that are produced in neutron interactions. Therefore, shielding materials are used in the divertor targets to protect vital components in the toroidal hall and to recover part of the energy carried by streaming radiation.

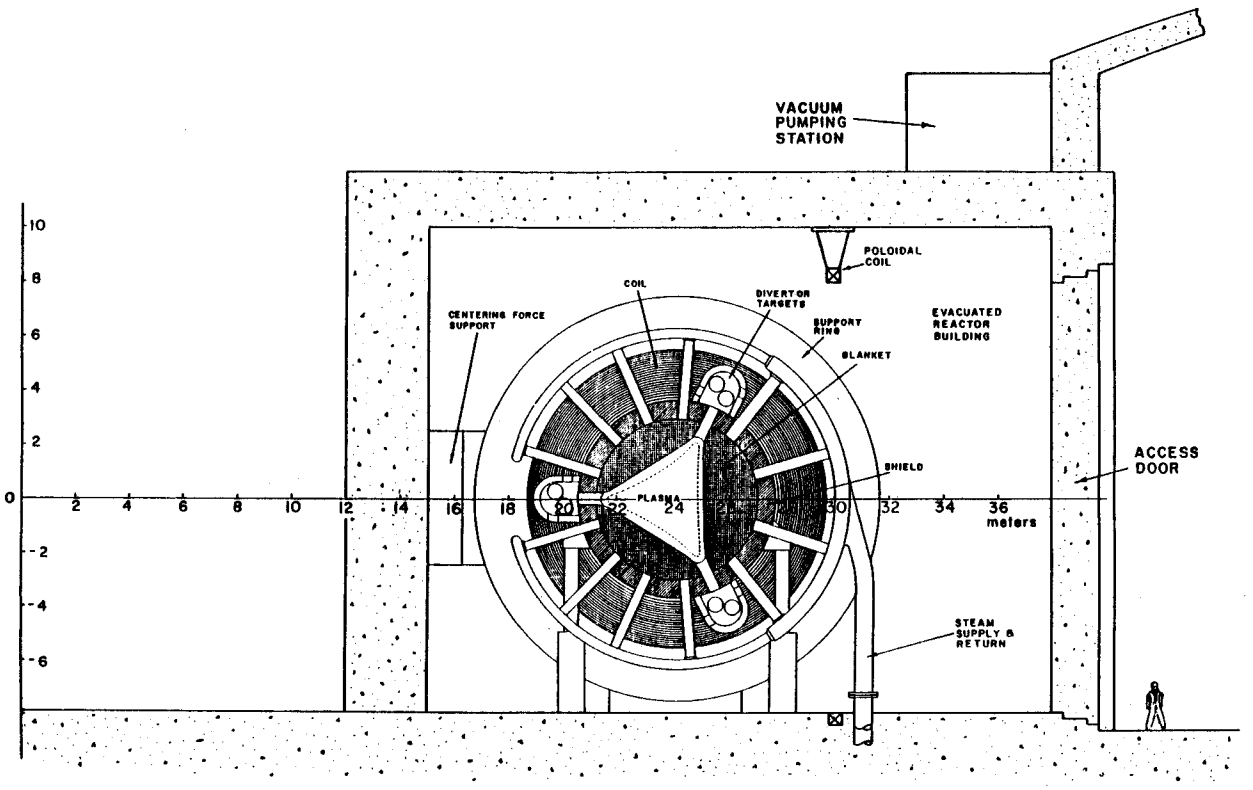

Fig. 1 Vertical Cross Section of UWTOR-M Reactor

The blanket design is aimed at achieving the largest energy multiplication with adequate tritium breeding. The Monte Carlo code MCNP with data based on ENDF/B-V was used to determine the proper blanket design. The effect the Li enrichment in the $Li_{17}Pb_{83}$ breeder has on radiation streaming was investigated. The streaming of down-scattered neutrons and secondary gamma rays increases as the enrichment decreases because of the decreased blanket attenuation. The results show that in the space available for the blanket the largest M that can be obtained is 1.15. This is achieved by using a Li enrichment of 35% and structural content of 9 v/o HT-9 in the blanket. The corresponding BR is 1.08.

Magnet shield optimization was performed using the discrete ordinates code ONEDANT to design a shield which provides adequate protection for the superconducting magnet utilizing the limited shielding space available. The shield consists of water cooled layers of Fe 1422, B_4C and lead. Among the different magnet radiation limits, the 10^{10} rad dose limit in mylar superinsulator in front of the magnet was found to drive the shield optimization as other magnet components are further protected by a 25 cm structural case.

The radiation streaming calculation procedure was divided into two parts by modelling the geometrical configuration of the reactor in two separate problems using MCNP. The blanket, reflector, and shield are considered as one problem and the divertor targets and associated shield as the other. Trapping surfaces were located at the entrance of the three divertor regions where all particles crossing the surfaces are counted according to angle and energy bins. This information was then stored to serve as a surface source in latter modelling of the divertor region itself. For each D-T fusion event, the total neutrons and gamma photons streaming through the divertor slots are 0.214 and 0.024, respectively, carrying a total power of 176 MW which represents 5% of the neutron fusion power. Fortunately, most of this energy is recovered by the divertor targets. About 20% of the streaming neutrons are primary neutrons and they carry 83% of the streaming energy.

The pumpout ports are located appreciably off the direct line of sight of the flowing particles from the divertor region entrance. This is of importance in reducing radiation streaming through ports. The results indicate that considerable attenuation and spectrum softening result from neutron interactions with divertor targets. The total power carried by radiation streaming through all pumpout ports of the reactor is 6 MW representing only 0.18% of the neutron fusion power. Radiation streaming raises the biological dose level outside the reactor. A 3.1 m thick toroidal tunnel wall made of reinforced ordinary concrete was found to result in an acceptable dose of 2.35 mrem/hr in the toroidal service hall during reactor operation.

In conclusion, despite the large radiation streaming through the divertor slots in a stellarator reactor, proper choice of blanket materials and composition can provide an adequate tritium breeding ratio and energy multiplication. High performance divertor targets can be used to intercept and recover most of the streaming radiation energy.

This work was funded by the United States Department of Energy.

VAPORIZATION OF Pb AND Li FILMS IN ICF REACTION CHAMBERS

A.M. Hassanein*, C.D. Croessmann, and G.L. Kulcinski
Nuclear Engineering Department, University of Wisconsin
Madison, Wisconsin 53706

The use of liquid Li and/or PbLi alloys have been recently proposed to protect ICF solid first walls from intense radiation following the explosion of a fusion target. The target spectra consist of neutrons, x-rays, and energetic ions but only the latter two pose a problem with respect to the melting of solid first walls. The liquid metals intercept the x-rays and ion debris at energy densities of 10-50 J/cm^2 which are deposited in times ranging from 10^{-8} sec for the x-rays up to 10^{-5} sec for the ion debris. The amount of Pb or Li which is vaporized by this radiation depends on several factors; the energy spectra of the x-rays and ions, the initial temperature of the liquid, and, of course, the power to the wall.

The code A*THERMAL has been used to compare the amount of Pb or Li that is vaporized from a wall 10 meters away from "typical" 175 and 350 MJ ICF target explosions. Two different target compressions were studied for each metal: ρR = 3 and 6 g/cm^2. The larger the initial compression of the target, the larger the energy in ions and x-rays, and hence the more radiation that must be handled on the first liquid surface. Figure 1 shows the temperature behavior of the exposed surface of liquid Pb for the two targets and it shows that the maximum temperature increase of the Pb varies by a factor of 1.5 between the two values of ρR. Figure 2 shows the difference in surface temperature of the Li and Pb film exposed to the same target spectra (ρR = 3 g/cm^2). It can be seen that Li does not have an initial temperature increase due to the x-rays because of its low absorption cross section.

For the case of ρR = 3 gm/cm^2, 1150 cm^3 (12 kg) of Pb is evaporated and for Li 2200 cm^3 (1.1 kg) is vaporized. More information on the target spectra and thermal response of the liquid will be included in the paper.

*Present address at Argonne National Laboratory.

Figure 1

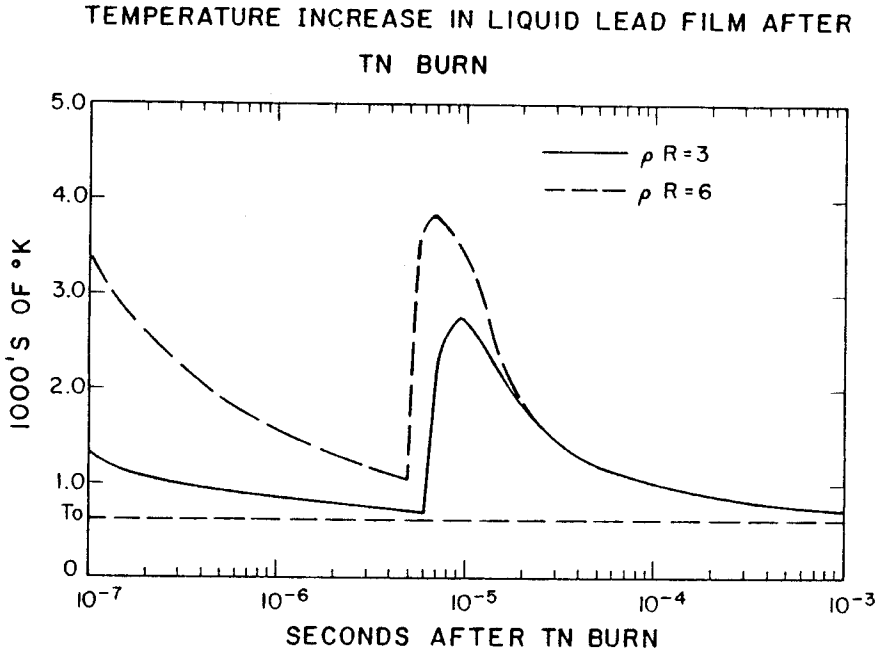

Figure 2

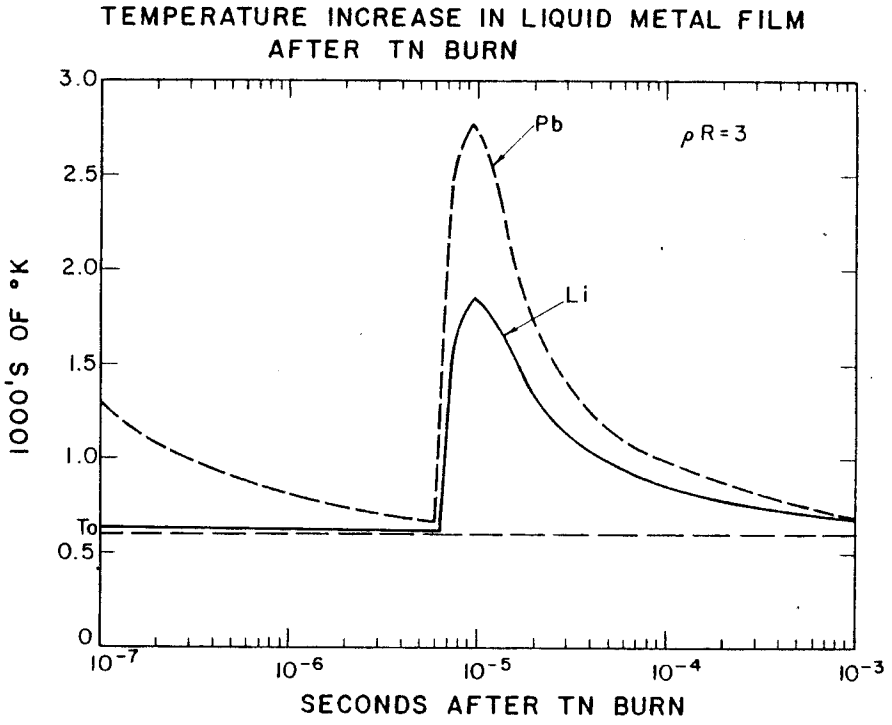

DYNAMIC RESPONSE AND STABILITY OF INPORT TUBES IN ICF REACTORS

Roxann L. Engelstad
Edward G. Lovell
University of Wisconsin - Madison

A persistent problem in the development of inertial confinement fusion reactors is protection for cavity structural walls from target debris, X-rays and neutrons. For this purpose a novel design has been proposed for the heavy ion beam fusion reactor HIBALL, a conceptual design jointly developed by the UW Fusion Engineering Program and the Kernforschungszentrum Karlsruhe, FRG. As shown below, the general configuration of the reactor chamber is cylindrical with the cavity first wall masked by an annular tube bank through which liquid $Li_{17}Pb_{83}$ flows. Individual

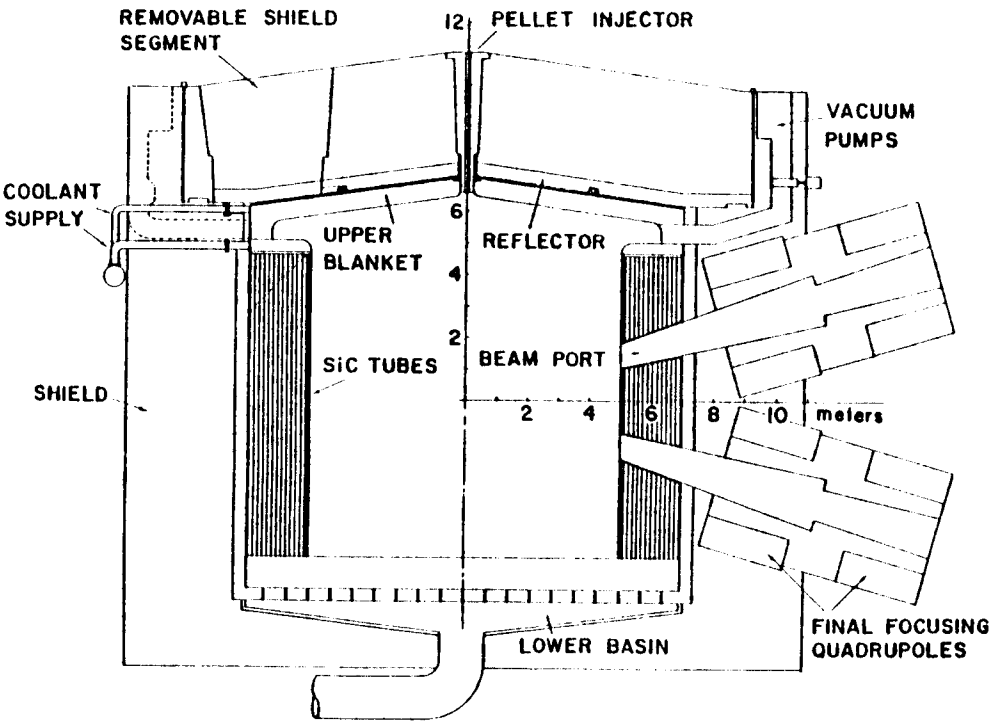

tubes, named INPORT units (Inhibited Flow/Porous Tube), are fabricated of porous woven SiC. Liquid LiPb flows primarily through the units, but with the wall porosity a protective layer (1 mm thick) is formed on the surface. This layer protects the INPORT by absorbing target debris and X-rays. Film vaporization from this energy deposition produces a reactive impulse on the tube. This paper is concerned with the response and stability of SiC tubes from this loading.

Analysis of the mechanical response of the INPORT units involves both stiffened and unstiffened tubes. In the former, the woven tubes are rigidized by chemical vapor deposition of SiC. Such members resist

transverse loading by flexural action, similar to structural beams. A general formulation is developed for natural frequencies, stresses and deflections including the effects of the LiPb flow. For uniform impulsive pressure, design data is presented which identifies the mechanical characteristics of these elements. Unstiffened tubes require separate analysis since these units resist lateral loading by tensile force action alone, i.e., having negligible shear and bending resistance. For the dynamic response, two support modes are considered. The first involves suspension from the upper end with the lower free to move while the second has the bottom end constrained in addition. For an impulse of 600 dyne-sec/cm^2, displacements are found to be quite large for single suspension, but acceptable for two point suspension. The results shown are for sequential impulses applied at 5 Hz.

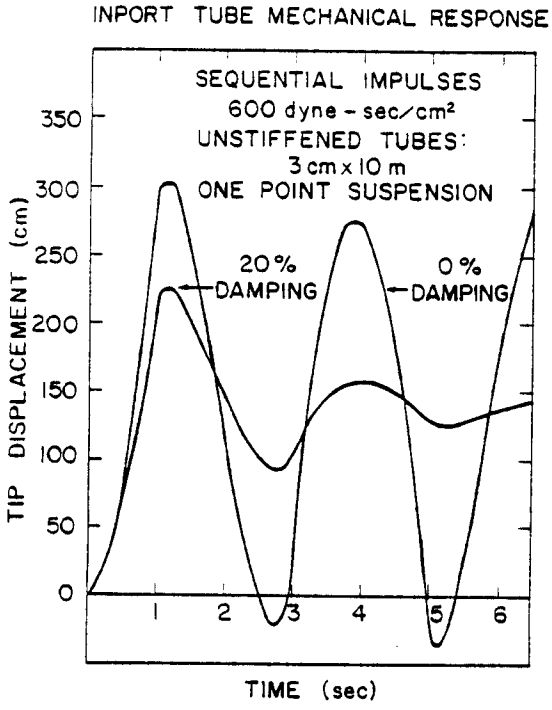

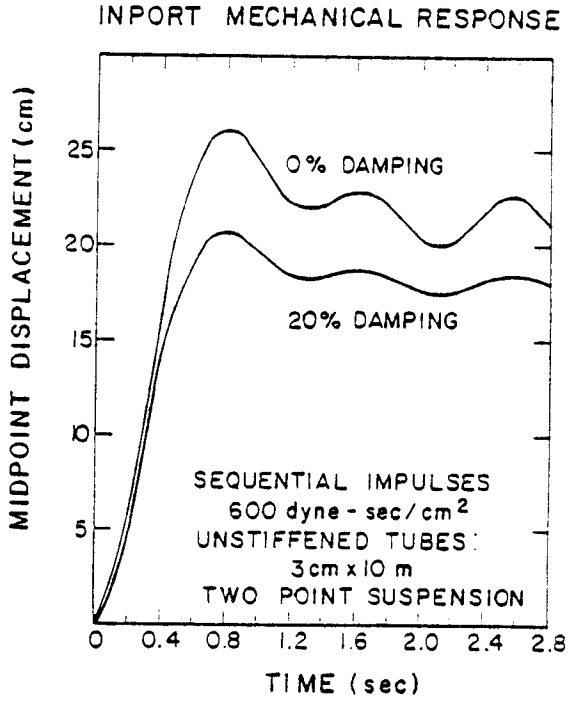

Forced vibrations produce another response of the INPORT units - nonplanar motion. When the tubes are driven by a force near the fundamental frequency, large amplitude oscillations become unstable and the tube displays a component of vibration in a direction perpendicular to the plane of the force. In essence, the tube begins to whirl, tracing a tubular path. Amplitude-frequency relationships are determined for both planar and nonplanar motion, showing regions of instability.

The analysis of the INPORT units shows that the vibration and deflection characteristics are generally compatible with the HIBALL design. The results identify the feasibility of the concept and guide the design for tube placement and their mechanical assimilation in ICF reactors.

AVAILABILITY ANALYSIS OF FUSION POWER PLANTS

Z. Musicki and C.W. Maynard (University of Wisconsin)

The purpose of this work is to assess the operational availability of future fusion power plants and its impact on the economics of electricity production, and to suggest design changes for improvement.

The present fusion power plant designs have many parts that have not been tested or built full scale. The sheer complexity and quantity of these engineering systems will present reliability problems.

If availability of such plants is low, their operation may prove uneconomical compared to alternative energy sources; the utilities will have to increase capital costs and must buy replacement power to offset this low availability. Increasing the availability (e.g. through redundancy), however, may entail increased capital costs.

A computer program has been developed which can be used to:

1) calculate approximate availability of a given design, or calculate a "worst case" and a "best case" availability.

2) compare different designs or different power plant concepts (e.g., mirror vs. tokamak) from the availability and economics standpoint.

3) suggest improvements in design for optimum cost of electricity. This economic optimum exists, because availability can be increased at the expense of increased capital costs.

4) identify the parts of a power plant that are availability drivers. Employment of availability drivers in power plants may then be minimized or resources can be concentrated on such components to bring about a reduction in their failure rates and repair times.

5) "apportion" failure rates and repair times for the subsystems so that an overall availability can be achieved.

The computer model for availability analysis uses the Monte Carlo approach to assess availability of each subsystem in a power plant. The subsystems are then combined in a logic diagram of the power plant (using logic gates) to find the availability of the whole plant. An economic model is employed to find the cost of electricity. The model can handle redundancy, m-out-of-n operation, maintenance timelines, limited maintenance facilities, idle operation, etc. It can also be made to handle transient analysis and aging of components if the need should rise and if appropriate data can be found.

There are obvious difficulties in obtaining the necessary data (failure rates and repair times) for the computer program input. Several avenues of approach have been considered:

- use data already available from industrial experience (e.g., pumps, steam generators).

- use data for analogous components (e.g., use accelerator data for neutral beam ion source).

- find data in design studies (STARFIRE, ETF availability apportionment, etc.)

- solicit data from the workers in the field who are familiar with certain subsystems and who may have a sense as to which numbers are reasonable and what are the uncertainties involved.

Using these sources, one ends up with the "best guess" data, as well as reasonable worst case and best case scenarios.

A study has been made on the UW-designed WITAMIR-I mirror reactor. Depending on design modifications, a range of availabilities between 18% and 35% has been computed. The availability drivers with the most significance are the magnets (especially the central cell coils) followed by the neutral beam injectors and ECRH system. Adding an extra central cell coil for online redundancy increases the availability and reduces the busbar cost of electricity by 30%, hence this addition is justified. In another study, a preliminary design of the MARS reactor, decreasing the failure rate of plug magnets by an order of magnitude improves availability from 16% to 20%. Halving the repair time of neutral beam injectors or ECRH increases the availability to 30%. Tokamak reactors are expected to have similar availability problems.

These numbers do not represent what we believe is truly achievable in fusion. We intend to show that improved design, quality control and maintenance procedures can lead to acceptable availabilities for both mirror and tokamak reactors.

In conclusion, a Monte Carlo computer code has been devised to calculate the availability of a power plant, given the logic interconnection of the subsystems in it. This computer code can handle redundancy, m-out-of-n operation and both scheduled and unscheduled maintenance. The calculated availability is incorporated into the economics code to compute the busbar cost of electricity. This can be used in comparison studies of different designs and reactor concepts. Availability drivers can also be identified.

In preliminary runs for the recent mirror reactors, a 20-30% availability has been calculated and magnet coils and neutral beams and ECRH system have been identified as availability drivers.

Acknowledgment

Support for this work has been provided by Wisconsin Electric Utilities Research Foundation and the U.S. Department of Energy.

MODELLING OF LITHIUM-LEAD/WATER INTERACTIONS

M.L. Corradini and D.K. Sze
University of Wisconsin
Nuclear Engineering Department
Madison, Wisconsin 53706

It is recognized that a molten metal can interact with water in such a way as to produce hydrogen and an accompanying release of mechanical energy. However, the magnitude of the interaction is highly dependent upon the metal composition, its temperature and mass, and the mode of contact between the metal and water. One of the efforts of the current fusion design project at Wisconsin[1] is to quantify the magnitude of the lithium-lead/water interaction that might occur in the blanket of the fusion power reactor, in the metal-water steam generator, or in the accompanying primary coolant loop and containment. One should realize that because some of the physical processes involved with molten metal-water interactions are not fully understood, our current analysis is scoping in nature and should be verified by experiments and more detailed analysis. The purpose of this paper is to present models for liquid-metal/water interactions to aid in understanding current data.

There have been scoping experiments performed by Clemmer, et al.[2-4] at Argonne National Laboratory and by Jeppson, et al.[5] at HEDL using lithium and lithium-lead alloys as the molten metal is poured into a water-pool. The results of the experiments have indicated that molten lithium-lead (i.e., 17Li83Pb) undergoes a qualitatively more benign reaction than lithium. There are two physical processes that are involved in a metal-water interaction:

(1) Physical explosion (also called vapor explosion or fuel-coolant interaction) where the hotter liquid (molten metal - "fuel") mixes with the colder liquid (water - "coolant") rapidly producing high pressure steam as the fuel is finally fragmented.
(2) Chemical reaction and burning when the molten metal which mixes with the water undergoes exothermic oxidation and produces hydrogen gas and the hydrogen burns.

The reasons why such a difference may exist is not completely known at this time. In this paper we investigate three possible reasons:

(1) The relative temperature rise for the lithium-lead alloy (17Li83Pb) is smaller than for molten lithium during oxidation.
(2) The lower reaction temperature coupled with realistic chemical kinetics produces slower reaction rates.
(3) The surface area available for reaction is probably smaller for the lithium-lead alloys.

We discuss each reason briefly in this summary.

The relative temperature rise for a 17Li83Pb-water chemical reaction is lower than for lithium. If one computes the thermodynamic maximum reaction zone temperature derived from a stoichiometric reaction of one mole of lithium and water, one finds that the maximum temperature is ~ 4350 K for lithium and ~ 1750 K for 17Li83Pb. The major reason for the difference is the large thermal inertia of the lithium-lead alloy.

This difference in the reaction zone temperature manifests itself in the chemical kinetics of the reaction. As the reaction zone temperature increases, the process of vapor phase oxidation becomes more dominant. Vapor phase oxidation occurs when the molten metal temperature increases to such an extent that the metal vapor pressure rises and metal vapor diffuses toward the water vapor and oxidation occurs. The vapor phase reaction kinetics are much more rapid than the liquid-metal/water reaction because the protective oxide layer on the metal surface does not inhibit the vapor phase reaction. For lithium at ~ 4350 K the partial pressure is ~ 10^5 torr, whereas for 17Li83Pb at 1750 K the lithium partial pressure is ~ 1 torr (the Li activity in 17Li83Pb is 10^{-3}). This suggests that vapor phase oxidation would be much less of a concern for 17Li83Pb. In fact, if one uses data from sodium-water reactions, vapor phase oxidation becomes dominant when metal vapor partial pressure rises above 100 torr. This analogy suggests that vapor phase oxidation is not a concern with 17Li83Pb.

In the absence of vapor phase oxidation the kinetic rate of reaction per unit area of a molten metal in water (i.e., steam because of film boiling between the metal and water) is controlled by the rate of steam diffusion to the metal surface and the rate of diffusion of oxygen through the oxide surface layer into the liquid fuel phase. Although the kinetics of the lithium-lead alloy reaction have not been measured, we believe that the rate of reaction would be lower than pure lithium for two reasons. First, the chemical activity of 17Li83Pb is much lower than lithium. Second, the rate of reaction would be reduced because the lithium would be more quickly depleted near the surface of the metal for lithium-lead because of its low mole fraction (17 a/o).

Finally, the total rate of oxidation is the product of the kinetic rate per unit area and the total molten metal surface area. Based on current research in fuel-coolant mixing with a drop or pouring mode of contact,[6] it appears that the rate of mixing and, therefore, the rate of fuel surface area generation is given by

$$\frac{dA_f}{dt} \sim \frac{6V_f}{C_o D_f} \qquad (1)$$

where A_f = fuel surface area
V_f = fuel volume
D_f = initial fuel diameter (length)
t = time
v_f = fuel relative velocity
ρ_c/ρ_f = density ratio of coolant to fuel

$$C_o \equiv \left(\frac{t}{T^+}\right) \exp\left(-T^+\right)$$

$$T^+ = \frac{tv_f}{D_f}\left(\frac{\rho_c}{\rho_f}\right)^{1/2}$$

Notice that as the coolant to fuel density ratio decreases (as would be the case for 17Li83Pb) the rate of area generation decreases. Slower mixing and area generation implies less surface area available for chemical reactions. Therefore, mixing takes ~ 3 times as long for 17Li83Pb than lithium. These results should be verified by experiments with simulation molten metals and water.

In summary, it appears that the rate of chemical reaction of lithium-lead is qualitatively less than lithium. In the paper we detail the specific models that one might use to quantitatively assess this difference. Further analysis will be presented in the paper discussing specified modes of contact and accidents for a particular fusion design.

References

1. B. Badger, et al., "MARS - Mirror Advanced Reactor Study", Interim Report, to be published, 1982.
2. R.G. Clemmer and D.R. Armstrong, et al., "An Experimental Study of the Reaction of Li_7Pb_2 With Water", Trans. Am. Nucl. Soc., 32, 71 (1979).
3. R.G. Clemmer and D.R. Armstrong, et al., "The Reactions of Li-Pb Alloys With Water", Trans. Am. Nucl. Soc., 34, 55 (1980).
4. A.G. Rogers and B.L. Benedict, et al., "Liquid Li-Pb-Bi, A New Tritium Breeder", Eng. Fusion Research Proc., Chicago, October 1981.
5. D.W. Jeppson and R.F. Keough, "Fusion Reactor Blanket and Coolant Material Compatibility", Proceedings of the Second Topical Meeting on Fusion Reactor Materials, Seattle, WA (August 1981).
6. M.L. Corradini, "A Proposed Mode for Fuel-Coolant Mixing", Trans. Am. Nucl. Soc., 41, p. 405, Los Angeles (1982).